Nanoscale Advances

ROYAL SOCIETY OF CHEMISTRY

REVIEW

View Article Online
View Journal | View Issue

Cite this: *Nanoscale Adv.*, 2022, **4**, 2608

Review on LSPR assisted photocatalysis: effects of physical fields and opportunities in multifield decoupling

Sijia Lv,† Yanping Du, †* Feitong Wu, Yichong Cai and Tao Zhou

Since nano scale local surface plasmon resonance (LSPR) can broaden the visible absorption region, enhance the local electromagnetic field and produce a thermal effect simultaneously, the appropriate utilization of the LSPR effect is a noteworthy research direction towards visible light driven photocatalysts with high efficiency and low cost. In this study, the influence mechanism of the optical, electric, magnetic, and thermal physical fields on the photocatalytic efficiency of the LSPR system is for the first time reviewed, based on which the research bottlenecks of this method including the accurate predesign and regulation of the photocatalyst, the interpretation of electron movement and energy transfer mechanism, are specifically analyzed. Due to the micro-nano localization of LSPR, auxiliary methods are needed to reflect the micro electromagnetic and temperature field distribution which are otherwise formidable to measure experimentally. Alternatively, numerical methods with decoupling calculations of nano-scale physical fields are necessary to develop. Therefore, the development potential of different numerical simulation methods including mainstream FDTD, FEM and DDA is subsequently expounded, providing opportunities in resolving the bottleneck issues associated with photocatalysis. It is worth mentioning that although many important advances have been achieved in the preparation and application of LSPR assisted photocatalysts, the convincing function mechanism of LSPR is still lacking due to its multifield synergistic enhancement effect.

Received 3rd March 2022
Accepted 28th April 2022

DOI: 10.1039/d2na00140c

rsc.li/nanoscale-advances

1 Introduction

Photocatalysis technology has been one of the hot spots in the field of frontier science because of its potential applications in energy, environment and health. So far, the two most important issues restraining the efficiency of photocatalysis have not been fundamentally solved:[1–4] (1) the high band gap of the photocatalyst. For example, the semiconductor TiO_2 has a band gap of 3.2 eV, which can merely be excited and undergo an electronic transition by light with a wavelength less than 387 nm. As a consequence, only the band beyond ultraviolet light fulfils the requirements for the excitation of electrons, which implies the utilization of a small proportion of solar light, leading to a relatively low photocatalytic efficiency. (2) The recombination

China-UK Low Carbon College, Shanghai Jiao Tong University, Shanghai, 201306, China. E-mail: yanping.du@sjtu.edu.cn
† These authors contributed equally.

Sijia Lv, candidate for a Master's degree at Shanghai Jiao Tong University. Her research interests mainly focus on multifield decoupling of LSPR-assisted photocatalysis.

Yanping Du, Associate Professor at Shanghai Jiao Tong University. He worked as Acting Project Leader at CSIRO and served as a guest editor of Frontiers in Energy Research. His research mainly focuses on high-efficiency heat storage, solar photothermal utilization, and the ultra-high heat flow cooling mechanism and application.

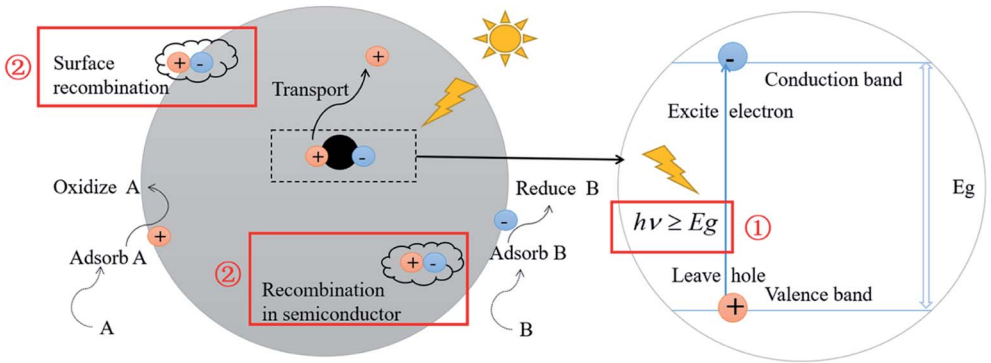

Fig. 1 Schematic illustration of semiconductor photocatalysis and its two most important restraining factors.

of photogenerated electron–hole pairs. This is ascribed to the short lifetime of the excited electrons and holes. As a result, most of the excited electrons and holes can't move to the surface of the particles to react, which severely decreases the efficiency of photocatalytic reactions. The above restraints in photocatalysis are schematically illustrated in Fig. 1.

The application of nano materials can significantly improve the photocatalytic performance of the system. On one hand, the nano size is beneficial to improve the charge transfer rate due to the shortened transportation distance. In 1995, Hagfeldt *et al.*[5] found that the diffusion time for electrons from the body to the surface of TiO_2 particles with a size of 1 μm was around 100 ns, while it decreased to approximately 10 ps when the particle size was reduced to 10 nm. On the other hand, the proportion of surface atoms can be increased apparently in some nano semiconductor particles due to the surface effect. For example, when the particle size of CdTe is reduced from 10 nm to 1 nm, the proportion of surface atoms can be increased from 11.4% to 70.6%.[6] Consequently, these surface atoms, lacking the adjacent atoms, show improved chemical and catalytic activity owing to their unsaturated bonds and dangling bonds with insufficient coordination. However, the fast recombination of photogenerated electrons and holes should also be taken into consideration for nano materials as the recombination process ($\sim 10^{-9}$ s) is considerably faster than the surface redox processes (10^{-8} to 10^{-1} s).[7]

Apparently, in the premise of nano-scaled catalysts, the optical, electric, magnetic, thermal and other physical properties of particles show distinct features compared with those in the macro size. For example, the quantum effect may appear in the particle size range of 1–10 nm, and the resulting physical properties are neither those of the bulk material nor those of molecular compounds. The quantum-mechanical rules lead to the broadening of the band gap and the blue shift of the absorption band, which means narrowing of the light absorption range. Nevertheless, the redox potential of the generated

Feitong Wu received her bachelor's degree in Nuclear Engineering and Nuclear technology from Shanghai Jiao Tong University, and her master's degree in Power Engineering from Shanghai Jiao Tong University, where her research field is photocatalysis.

Yichong Cai received his bachelor's degree from Jilin University in 2020 and is pursuing his master's degree at Shanghai Jiao Tong University. His research focuses on composite photocatalysis based on Au plasmons and visible light-driven CO_2 photocatalytic methane production.

Tao Zhou, a PhD candidate at the School of Mechanical and Power Engineering, Shanghai Jiao Tong University. His research mainly focuses on heat storage based on phase change materials, photocatalytic reduction of carbon dioxide, the design of composite-based catalysts, fundamental studies of catalyst structures and catalytic reaction mechanisms.

carriers is simultaneously improved due to the enlarged band, resulting in the potential augmentation of the catalytic activity.[6] Interestingly, it has been proven that the quantum effect can also cause the local surface plasmon resonance (LSPR) of metal nanoparticles (NPs), which is of significance to be considered for better utilization of sunlight.[8–12]

For the metal nanostructures with the LSPR effect, a strong resonance absorption peak occurs when the oscillation frequency of the electrons is consistent with the frequency of the incident light wave, as shown in Fig. 2.[13] The dopant perturbation of the semiconductor electronic structure and the resultant increase in the electron density at the Fermi level are indicated as the likely cause for this strong LSPR absorption.[14] Chou *et al.*[15] prepared the Au NP-modified ZnO composite films deposited on ITO glass. The LSPR effect of Au NP solutions shows an obvious peak of absorbance which is located at 519 nm. However Kominami *et al.*[16] loaded Au NPs on TiO_2, exhibiting photoabsorption due to LSPR at around 620 nm. The apparent quantum efficiency reached 7.2% at 625 nm and 4.2% even at 700 nm. Based on these excellent optical absorption properties of the LSPR effect, many scholars put great efforts in addressing the issue of high band gap of traditional semiconductors and broadening the photoresponse range by using LSPR-assisted (such as Au,[17] Ag,[18] Fe,[19] and Cu[20]) photocatalysts. For example, it was demonstrated that catalytic reduction of CO_2 can be achieved over Au NP deposited TiO_2 under full solar-spectrum irradiation, thanks to the absorption peak at around 580 nm in the visible range caused by the LSPR effect of Au NPs.[17] Similarly, the visible-light-induced photocatalytic degradation of polycyclic aromatic hydrocarbons was achieved by using Fe-doped TiO_2. To further specify the reasons for the extended absorption edge from ultraviolet toward the visible region, Fe-doped TiO_2 and undoped TiO_2 were investigated by using UV-Vis diffuse reflectance spectra. The results showed that the presence of Fe(III) reduced the bandgap energy of TiO_2 (3.2 to 2.67 eV) due to the electron transition from the 3d Fe energy level to the TiO_2 conduction band.[19]

More importantly, the optical properties of these plasma nanomaterials are highly controllable in the whole visible light range. The common methods are as follows: firstly, experiments have shown that the absorption peak can be shifted by changing the content of metal NPs in the photocatalyst system. For example, Podlipensky *et al.*[21] studied the absorption spectra of Ag NP composite glass with different volume fractions, as shown in Fig. 3a. The results showed that with an increase of the volume fraction, the interaction between Ag NPs caused the resonance absorption peak to move in the long wave direction, resulting in a wider absorption range. However, in Ni and Ag implanted SiO_2 nanomaterials,[22] the shift direction of the LSPR peak tended to be opposite, which implied a blue shift with the increase of the Ni content. Secondly, some scholars changed the optical properties of LSPR nanomaterials by designing specific microstructures such as cavities[23] or core–shells,[24] which could be adjusted continuously in the fabrication process. Yue[23] prepared Au–Ag alloy NPs with controllable cavity sizes (35 nm to 20 nm). As a consequence, the LSPR peak was continuously adjusted between 490 nm and 713 nm. Compared with single TiO_2, the photocatalytic hydrogen production rate of Au–Ag NPs/TiO_2 increased from 0.48 μmol h^{-1} to 4 μmol h^{-1}. Lin[24] prepared the Au@SnO_2 core–shell structure as shown in Fig. 3b. The experimental results indicated that the red shift of plasmon resonance absorption could be continuously achieved by increasing the size of Au NPs or the thickness of the SnO_2 shell. Also, rod-shell and sphere-shell structures showed distinct optical properties due to different resonance modes. Thirdly, the light absorption can also be regulated by changing the size and shape of metal NPs.[25–28] It was experimentally found that with the increase of the particle size, the surface plasmon absorption of spherical Au NPs red shifts continuously, and the resonance absorption range is widened.[25] Peng[26] and Jiao[27] both investigated the influence of shape factors on the resonance absorption of LSPR. Peng[26] adjusted the LSPR peak by changing the aspect ratio of Al NPs, as shown in Fig. 3c. Similarly, Jiao[27] prepared Au/Pt core–shell NPs to examine the effect of the aspect ratio of Au nanorods on the regulation of the LSPR absorption peak. It was reported that the longitudinal absorption peak of Au was continuously adjusted from 520 nm to 955 nm. Additionally, in Pang's study,[28] the plasmon NPs are of equal volume and height but had different shape factors. It was found that the resonance absorption moved to the long wave

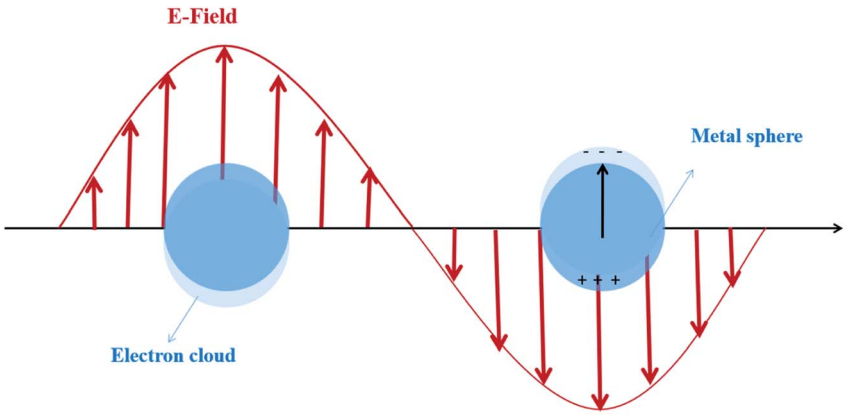

Fig. 2 Local surface plasmon resonance excitation. Reprinted from ref. 13. Copyright 2014, ACS.

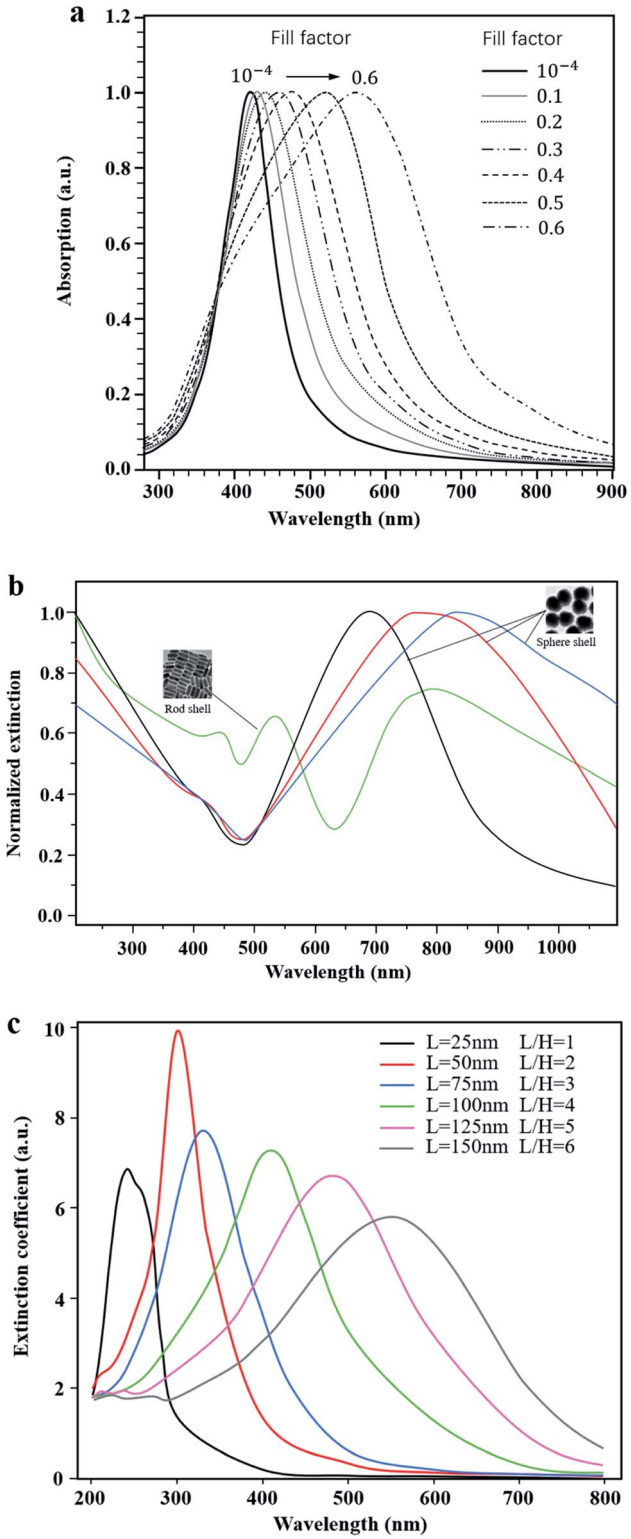

Fig. 3 Highly controllable optical properties of LSPR. (a) Absorption spectra of composite glass with different contents of Ag nanoparticles. Reprinted from ref. 21. Copyright 2005, Springer. (b) Normalized extinction of Au@SnO_2 with varying structures. Reproduced with data source from ref. 24. (c) Extinction coefficient spectra of Al NPs of different sizes. Reproduced with data source from ref. 26.

direction and had extended resonance absorption when the particle shape varied from circle to ellipsoid, square, diamond, fan and triangle, respectively.

Due to the LSPR effect, the local electromagnetic field on the surface of the metal NPs (extending tens of nanometers outward from the surface) will also be significantly enhanced. Theoretically, the stronger the electromagnetic intensity is, the more photogenerated electron–hole pairs can be potentially separated. From the experimental point of view, He[29] constructed a Ag/AgX composite photocatalyst for the photoreduction of CO_2. Consequently, the production of CH_4 in 1 hour was improved by 28.7 times. The enhancement of photocatalytic activity could be attributed to the increased separation velocity of electron–hole pairs and the close-range dipole–dipole resonance at the interface between the semiconductor and metal due to the enhanced local electromagnetic field. It was pointed out that the electrons excited in the semiconductor were mainly located in the shallow position below the surface, allowing an extremely short diffusion distance to the surface. Therefore, thanks to the enhanced local electromagnetic field, electron–hole pairs could be rapidly generated near the semiconductor surface and promptly migrate to the surface to have oxidation/reduction reactions.

In addition, LSPR can also produce thermal effect. Chen *et al.*[30] established a heat transfer model for Au NPs immersed in water based on the finite element method, and studied the heating and shaping of Au NPs induced by nanosecond pulse light. The model showed that the temperature of Au NPs could increase from room temperature to above 795 K in a few nanoseconds under the conditions of low brightness due to the enhanced light absorption by strong plasma resonance. Significant surface heating enabled the molecules to overcome the high potential energy barriers in chemical reactions,[31,32] which was beneficial to improve the photocatalytic reaction efficiency. Linic *et al.*[33] examined the influence of the thermal effect by LSPR. It was found that due to the LSPR effect of Au, Ag and Cu, the oxidation reaction rate driven by photothermal catalysis (mol h^{-1} g^{-1}) is much higher than that of the traditional photocatalysis (umol h^{-1} g^{-1}).

Except for the significant effect of a single physical field on the photocatalytic efficiency, the coupling of multiple physical fields also leads to many special phenomena in photocatalytic systems. For example, it has been confirmed that the photothermal catalysis[34,35] can significantly improve the catalytic performance. Wei *et al.*[34] systematically collected 65 types of catalytic systems from 1995 to now. Table 1 compares the performance of photocatalysis, thermal catalysis and photothermal catalysis in VOC degradation. The data showed that photothermal coupling could significantly improve the photocatalytic efficiency, which was much higher than that of single photocatalysis or thermal catalysis. Li[43] studied the combined effect of optical and electromagnetic fields on the photocatalytic efficiency based on nanostructured Co-doped $Bi_7Fe_3Ti_3O_{21}$ (BFTO), which shows both electric polarization and photocatalytic activity. As per their experiments, with the increase of Co doping in the BFTO lattice, the visible absorption and ferroelectric properties were largely enhanced, contributing to

Table 1 Summary and comparison of the performance of photocatalytic (PC), thermocatalytic (TC), and photothermal catalytic (PTC) degradation of VOCs[34]

			PC activity			TC activity			PTC activity			
Catalyst	VOC	Light source	T/°C	t/min	C/%	T/°C	t/min	C/%	T/°C	t/min	C/%	Ref.
Anatase TiO_2{001}	Benzene	Hg	RT	65	42	—	—	—	290	65	78	36
Rutile TiO_2	Benzene	UV	RT	160	50	280	160	18	280	160	70	37
TiO_2	Benzene	UV	40	60	40	240	60	15	240	60	100	38
0.1 wt% Pt/TiO_2	Benzene	UV	—	—	—	240	60	89	240	30	100	38
TiO_2	Benzene	Fluorescent black light bulb	—	—	—	140	300	30	140	300	86	39
0.1 wt% Pt/TiO_2	Benzene	Fluorescent black light bulb	—	—	—	70	120	8	70	120	100	39
0.1 wt% Pt/TiO_2	Benzene	Fluorescent high-pressure Hg	RT	30	22.1	—	30	47.3	—	30	100	40
0.5 wt% Pt/TiO_2	Benzene	UV	—	—	—	240	20	87.7	240	20	100	40
Pt/TiO_2/silica	Ethylene	UV	—	—	—	90	—	34	90	—	100	41
Pd/TiO_2/silica	Ethylene	UV	—	—	—	90	—	19.2	90	—	100	42
Au/TiO_2/silica	Ethylene	UV	—	—	—	90	—	4.5	90	—	94.9	42

the generation of carriers and its separation, respectively. However, due to the consequent recombination centers caused by the strong magnetism, the promotion on the photocatalytic effect was not as apparent as that in theory.

It is worth noting that the LSPR effect can broaden the spectral absorption range, enhance the local electromagnetic field and generate thermal effect simultaneously. The three main function mechanisms originating from the multi-field coupling processes are listed in Fig. 4.[44] Starting from mechanism A, hot electrons are created by visible absorption and then the catalyst is further activated by hot electron transfer from the plasmonic NP. At the very same time, the concentrated local electromagnetic field around the NP helps in electron–hole separation (mechanism B) and the thermal-induced reaction is improved by the temperature increase around the plasmonic NP (mechanism C). As a consequence, with this triple excellent characteristic, LSPR is regarded as an emerging technique to develop for next-generation photocatalysts.

Note that in the literature about LSPR-assisted photocatalysis, the function mechanisms of LSPR through the optical, electric, magnetic, and thermal physical fields are sometimes considered in isolation or the identification of the involved mechanism(s) might remain unclear, hence we systematically summarized the effect of physical fields on the photocatalytic efficiency in the next section of this review. The most attractive special phenomena caused by the synergistic enhancement of multi-fields are also covered especially. Since few scholars have considered the coupling between the four physical fields of LSPR assisted photocatalysis, the profound prospect of multifield decoupling is highlighted, as discussed in the last section of this review.

However, because of the microcosmic localization of the LSPR effect, it is difficult to measure the nano scale system directly. To overcome the difficulties in experiments, numerical tools can be used to examine the intrinsic properties of NPs in coupled physical fields, including the optical field, electromagnetic field and temperature field in the nanometer scale. This is meaningful for photocatalytic analysis since the evaluation of performance of the modified nano catalyst is mainly based on the absorption spectrum and the electromagnetic field intensity on the particle surface.[45–47] And the current numerical simulation software can basically realize the coupling calculations and visualization of multiple physical fields. Besides, the accuracy and reliability have also been proved by many simulation-experiment comparative studies.[48–50]

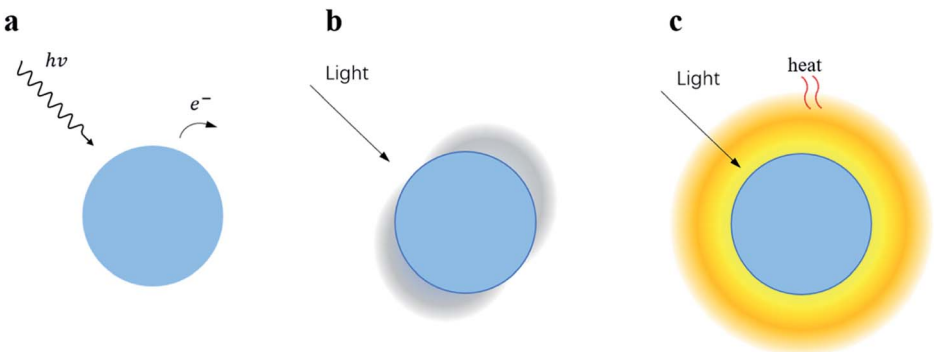

Fig. 4 Triple excellent characteristics of LSPR. Mechanism A: a photo-induced hot electron can be transferred from the NP under visible light. Mechanism B: the enhancement of the local electromagnetic field at the vicinity of the NP helps reduce the electron–hole recombination. Mechanism C: the photo-induced temperature increase of the NP provides heat to the reaction system. Reprinted from ref. 44. Copyright 2014, Chemical Society.

In this paper, we first discuss the influence of the optical, electrical, magnetic and thermal physical fields on the photocatalytic efficiency so as to highlight the excellent characteristics of LSPR. Subsequently, through reviewing the state-of-art literature on the physical fields of the photocatalytic system based on the LSPR effect, we point out the current bottlenecks of the LSPR assisted photocatalysis. On this basis, the development potential of numerical simulation methods (mainly three mainstream methods FDTD, FEM, and DDA) in this field is elucidated. For each method, the fundamental principles, key advances and unique advantages are presented in detail. Finally, the research prospect of multifield decoupling of LSPR assisted photocatalysis by numerical simulations is illustrated.

2 Effect of physical fields on photocatalytic efficiency

2.1 Optical absorption

Intrinsic absorption is a process in which an electron in the conduction band (CB) absorbs a photon and then transits to the valence band (VB). The occurrence of intrinsic absorption is the precondition of the catalytic reaction. The selective absorption of photocatalysts is crucial to be investigated due to its role in a highly efficient photocatalytic system.

Most semiconductor photocatalysts have large band gaps, thus the electrons in the valence band can be excited only under ultraviolet light. However, in sunlight, most of the energy is in visible light (45%) and infrared (52%) regions, and the energy of ultraviolet light only accounts for around 3% of the total energy received by the earth. The total efficiency of photocatalysis can be expressed as the product of the optical absorption efficiency, charge separation efficiency and surface reaction efficiency.

$$\eta_{\text{total}} = \eta_{\text{optical absorption}} \times \eta_{\text{charge separation}} \times \eta_{\text{surface reaction}} \quad (1)$$

Despite common modification methods including the heterostructure,[51–55] ion doping[49–55] and dye sensitization[56–62] (shown in Fig. 5), the low utilization of sunlight in the optical absorption severely restrained the improvement of the photocatalytic efficiency. Therefore, extending the optical response range from the ultraviolet region to the visible region is a major issue to overcome.

To realize the visible-light-driven photocatalysis, heterojunctions, constructed from two semiconductors with different band structures, have drawn much attention from scholars. Theoretically, if the two semiconductors possess different Fermi energy levels, the spontaneous diffusion of electrons is expected to occur from the semiconductor with the higher energy level to that with the lower one, consequently promoting the spatial separation of photo-excited electron–hole pairs. Based on appropriate design, these semiconductor composites provide a feasible means to achieve a good visible response. For instance, Zhao *et al.*[51] studied the composite catalyst CdS/TiO_2 core–shell structure and found that its light absorption range increased markedly. This is because the visible-photo-excited electrons of CdS migrate to the conduction band of TiO_2, so as to broaden the light response and increase the free electron concentration. In the application of photocatalytic performance improvement, Yang *et al.*[52] successfully fabricated carbon doped TiO_2 modified graphitic carbon nitride (C-TiO_2/g-C_3N_4) *via* a facile heat treatment in air. The optimized bandgap structure of this heterojunction conferred superior photocatalytic activities with 5.728 mmol g^{-1} photogenerated hydrogen gas for 5 h. Liu *et al.*[53] fabricated a CdS-g-C_3N_4-graphene aerogel heterojunction for enhanced visible light driven photocatalysis, which

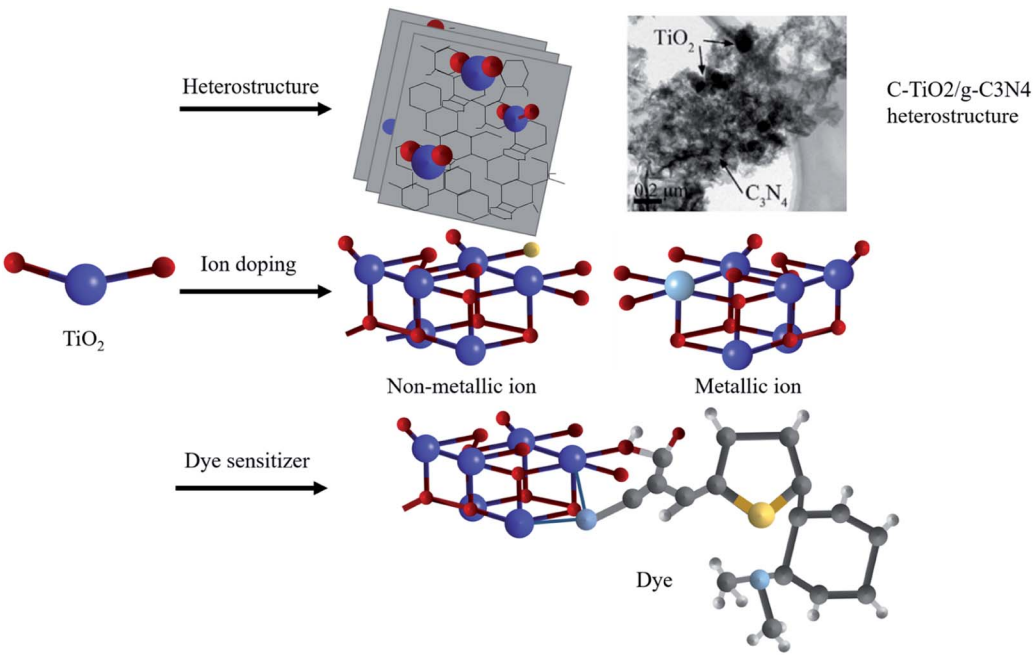

Fig. 5 Schematic illustration of modification methods: heterostructures,[52] ion doping and dye sensitization. Copyright 2017 Elsevier.

reveals greatly improved harvesting ability for solar energy. The photodegradation efficiency of RhB reached up to 91.4% within 50 min under visible light irradiation, which was about 40 and 11 times higher than that of pure g-C_3N_4 and CdS. For further reference, the bandgap energies and CB-/VB-edge energies of some important semiconductors calculated by Yang are summarized in Table 2.[54] However, at present, the heterojunction is difficult to prepare under experimental conditions owing to the practical doping technique and the establishing requirements of the proper bandgap structure.[54,66]

This stimulates the method of ion doping, which forms an intermediate band between the valence band and conduction band through the introduction of heteroatoms. Since it can respond to lower energy photons (visible light), ion doping also helps improve the efficiency of solar energy utilization. In 2001, Asahi *et al.*[67] published in Science and reported that they realized the absorption and utilization of visible light by preparing a nitrogen doped TiO_2 thin film photocatalyst. Subsequently, scholars further studied other non-metallic doped ions such as carbon (C), sulfur (S) and fluorine (F), and obtained similar results.[68–71] However, the existing results show that only non-metallic elements with a radius less than that of oxygen can partially replace oxygen atoms, and defects introduced by excess impurities might act as recombination centers, resulting in the decline of photocatalytic activity.[71] After that, some scholars used aluminum (Al), iron (Fe), gold (Au) and silver (Ag) as doped ions.[72] However, the photocatalytic activity is related to the relative position of the doped metal ions, which puts forward strict requirements for the selection of metal ions and the preparation process for material doping. Liu *et al.*[73] further clarified the similarities and differences in the reaction mechanism of metal and non-metal ion doping. They pointed out that the doping of metal ions would replace part of titanium atoms in the TiO_2 lattice, which might introduce defects in the TiO_2 semiconductor lattice or change the crystallinity. This would significantly affect the recombination of electrons and holes or prominently change the excitation wavelength, leading to the increase of the catalytic performance of TiO_2. However, in the case of non-metallic doped TiO_2, some oxygen atoms in the lattice are replaced. Due to the hybridization of the 2p orbital of oxygen and p orbital of non-metallic medium, the valence band is broadened, causing a reduced band gap.

Dye sensitizers are synthesized by incorporating dyes on the surface of semiconductor photocatalysts. Since the adsorbed dyes match the conduction band and valence band energy of the wide-bandgap semiconductor, the spectral response can also be extended to the visible region by using the dye-assisted photocatalysts.[74] As shown in Fig. 6a, after adsorbing visible light to reach the excited state, the electrons from the highest occupied molecular orbital (HOMO) of the dye are first transferred to the lowest unoccupied molecular orbital (LUMO) and then to the conduction band of the semiconductor.[75] Therefore, free radicals with higher concentration will be formed in the conduction band to further improve the photocatalytic efficiency. At present, the most widely-studied dye sensitizers are metal organic dyes[74,76] and synthetic organic dyes.[77] Zhou *et al.*[74] optimized the energy band structure of TiO_2 by using two zinc phthalocyanine dyes and increased the light response range. The excellent performance of co-sensitization of the two dyes in increasing the photocatalytic performance of TiO_2 was also examined in their study. Huang *et al.*[76] used SnHTPP to modify TiO_2 NPs and studied its photocatalytic activity. The experiments showed that the photocatalytic degradation rate of methyl orange could reach 86% under visible light irradiation. Khan *et al.*[77] investigated the degradation mechanism of the dye sensitizer consisting of synthetic organic dye eosin and TiO_2. Although the dye sensitizer has a positive effect in promoting the photocatalytic activity, the metal organic dyes may result in environmental issues and cause secondary pollution, while synthetic organic dyes have the disadvantages of low light conversion efficiency and weak chemical stability. Nevertheless, green and low-cost dye sensitizers, for instance, dyes extracted from plants, have high potential to be utilized as a substitute of conventional dye sensitizers ascribed to eco-friendly features and superior sensitization under a wide light spectrum.[78–80]

As can be seen from Fig. 6b and c, heterostructures, ion doping and dye sensitization modification methods are based on adjusting the energy band structure, thus each method has its specific improved range of light absorption. Different from the above methods, LSPR increases the light absorption efficiency by coupling the energy of incident light to the plasmon nanostructures under resonant excitation. Moreover, the strong resonance absorption peak is highly adjustable in the visible and near-infrared region, which makes the LSPR effect an ideal means to enhance the absorption and utilization of solar energy.

Zheng[81] summarized the performance of these modification methods on the TiO_2 catalyst and emphasized that compared with the heterojunctions, the LSPR assisted photocatalyst was relatively easy to be prepared. Besides, the LSPR effect can overcome the problems of shorter photocatalytic reaction life caused by dye sensitization and easy recombination of electron–hole pairs caused by metal ion doping. According to ref. 82 and 83 the absorption cross section of metal NPs is five orders of

Table 2 Bandgap energies and CB-/VB-edge energies of some important semiconductors[54a]

Semiconductors	Bandgap energy E_g (eV)	CB-edge energy E_C (eV)	VB-edge energy E_V (eV)
Co_3O_4 (ref. 55)	1.98	+0.44	+2.42
TiO_2 (ref. 56)	3.10	−0.24	+2.86
WO_3 (ref. 56)	2.61	+0.79	+3.40
ZnO[57]	3.37	−0.40	+2.97
α-Fe_2O_3 (ref. 58)	2.25	+0.27	+2.52
SnO_2 (ref. 59)	3.60	−0.05	+3.55
In_2O_3 (ref. 60)	2.35	−0.40	+1.95
MnO_2 (ref. 61)	1.76	+0.58	+2.34
AgBr[62]	2.70	−0.04	+2.66
AgI[63]	2.89	−0.47	+2.42
CdS[64]	2.40	−0.51	+1.89
CdSe[65]	1.73	−0.32	+1.41

[a] E_C^0 is defined as the energy of the conduction band at the point of zero charge.

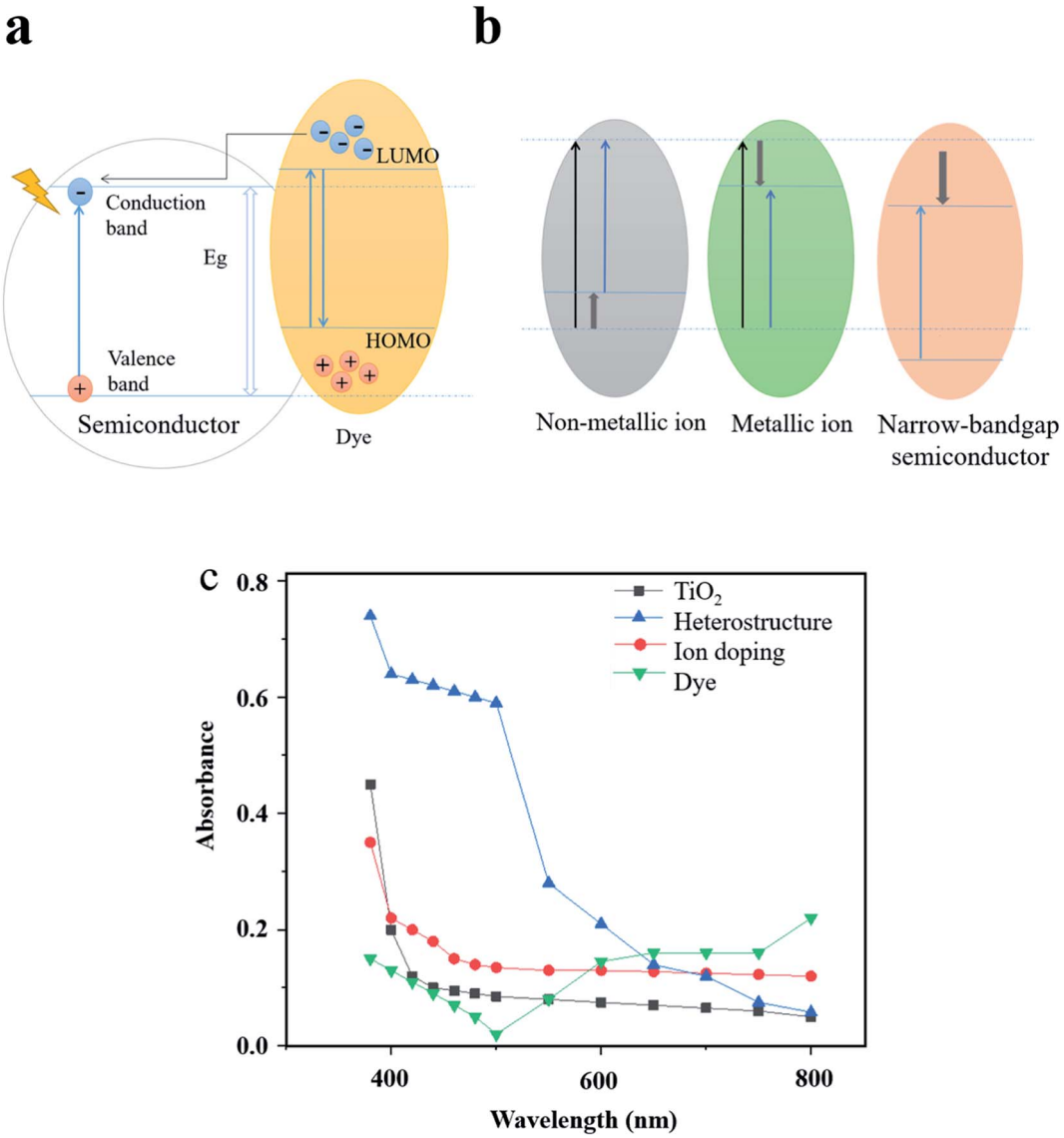

Fig. 6 Expanding the optical response range by adjusting the energy band structure. (a) Light absorption mechanism of dye sensitization as an example. (b) Energy band structure of different modification methods. (c) Comparison of the light absorption efficiency of typical modification examples. Reproduced with data source from ref. 51, 71 and 74.

magnitude larger than that of typical dye-sensitizer molecules, and their photocatalytic efficiency improvement is much higher than that of commonly used quantum dots, organic dyes and non-metallic ion doping.

Since the geometrical structures and light attributes may have a direct influence on the LSPR optical properties, investigating and understanding of the crucial parameters that affect the LSPR spectrum are important for the design and fabrication of LSPR devices. The important design considerations for metal NPs include the size effect, multi-particle interaction effect, sharp tip effect, aspect ratio effect, material effect and asymmetry effect. The effect of these parameters on dipole plasmon resonance including the wavelength shift and intensity enhancement rate is summarized in Table 3.[84] Besides, more and more advanced LSPR-assisted structures are proposed, such as the core–shell,[85–87] cavity array[88,89] and hollow nanostructures.[90–92] These strategies significantly contribute to the visible light-driven photocatalysis due to the optimized plasmon optical absorption.

However, current research studies on the design of the LSPR-assisted structure still have focus on the optimizing spectral characteristics of metal, without consideration of enhancement for a specified semiconductor.[93] This puts forward strict requirements for the accurate modulation of the plasmon absorption peak of metal NPs. Also, since the extinction spectrum can be controlled with careful design of nano-particle geometries and incident wave attributes, a predicted photocatalytic system in advance to better guide the subsequent preparation work is a necessity. Based on the above review, it is worth mentioning that the preparation of LSPR assisted

Table 3 Design parameters affecting the LSPR efficiency[84]

Parameters	Wavelength shift	Intensity enhancement rate
Intrinsic region size increase	Blue-shift	More enhancement
Tip sharpness increase (*p*-polarization)	Red-shift	More enhancement
Aspect ratio increase	Red-shift	More enhancement
Analyte permittivity increase	Red-shift	—
Asymmetry (defects) increase	Red-shift	More enhancement

photocatalysts with a low cost, high efficiency and precise control is probably the emerging trend for the promotion of photocatalytic activities and its realistic application.

2.2 Charge separation and energy transfer based on the electromagnetic field

In addition to the optical absorption, the charge separation is another critical factor that restrains the photocatalytic efficiency as shown in eqn (1), which attracted much attention to the electromagnetic field in photocatalytic reactions. The built-in electric field, which can be used as driving force to effectively control the migration behavior of carriers, is widely discussed in the recent first class of studies.

Some scholars successfully facilitate the built-in electric field based on nanosized heterojunctions.[94–96] As we already discussed, it is possible to realize the spontaneous diffusion of electrons between two semiconductors with different band structures. During this process, a consequent built-in electric field is expected to be formed at the heterojunction interface, so as to inhibit the geminate recombination of the carriers. Also, it is noted that the formation of the built-in electric field and the carrier transfer behavior between the constituent semiconductors depend on many factors, such as semiconductivity, Fermi level, and CB/VB potential of semiconductors.[54] In aspect of photocatalytic performance improvement, Chen *et al.*[94] constructed a $Mn_{0.5}Cd_{0.5}Se$ heterojunction to enhance the photocatalytic efficiency. The built-in electric fields contribute to a 7.2 fold increase in hydrogen evolution against pure CdSe. He *et al.*[95] developed controllable morphology $CoFe_2O_4$/g-C_3N_4 p–n heterojunction photocatalysts with the built-in electric field, which showed a high photocatalytic hydrogen evolution rate of 18.9 mmol g^{-1} h^{-1}.

The effect of the electric field is also profound in the LSPR-assisted photocatalyst. Following the law of Fermi–Dirac distribution, the electrons in the occupied states below the Fermi energy level, under incident light excitation, will be excited to the unoccupied states above the Fermi energy level. Because of the metallic nature of plasma, their electrons will become excited free carries, which can oscillate collectively with alternating external electromagnetic fields and thus generate an enhanced electromagnetic field.[97] Taking Au nanocluster decorated TiO_2 as an example, owing to the LSPR induced electric field amplification near the TiO_2 surface,[98] the photon absorption rate of Au-deposited TiO_2 visible light illumination for photoelectrochemical water splitting was enhanced by 66-fold.[99]

To further explain the significant the photocatalytic efficiency caused by the built-in electric field, two feasible mechanisms were proposed: one was the extended optical absorption capacity. Since photogenerated electrons could be forced to move through the built-in electric field according to the Fermi energy level, it is possible to produce visible-light-excited carriers by introducing a visible light-driven catalytic component into the catalytic system, typically the narrow bandgap (<2.5 eV) semiconductors or the metal NPs with the LSPR effect. The other is the high charge separation efficiency. Even though the amount of absorbed photons is restricted, promoted separation of electron–hole pairs may still bring more active carriers to take part in redox reactions. Both these two assumptions correspond with eqn (1).

The two mechanisms above are both able to function in heterojunctions and LSPR-assisted catalysts. More noteworthy, it was reported that the broadened spectral response and local electromagnetic field enhancement could occur in collaboration and promote each other in one intelligently-designed system.[100] For instance, this multifield synergistic enhancement mechanism is observed in Ag cluster-incorporated AgBr nanoparticles on TiO_2 (Ag@AgBr/mp-TiO_2) shown in Fig. 7.[101] Spectroscopic and photoelectrochemical measurements suggested that the high photocatalytic activity stems from the enhancement of the local electric field near Ag clusters

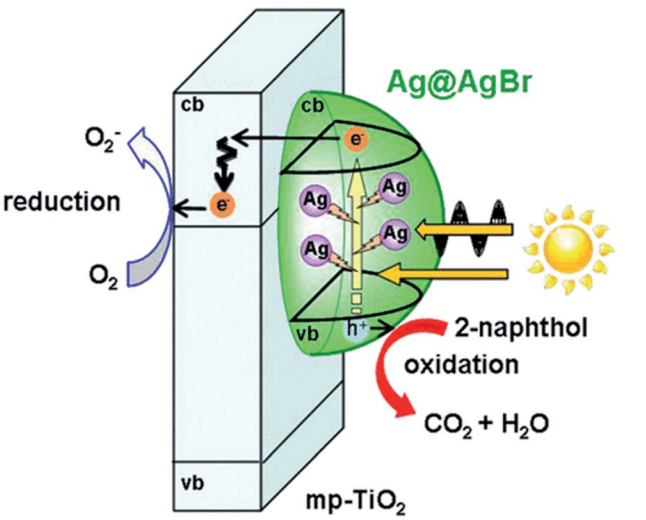

Fig. 7 Action mechanism of the Ag@AgBr/mp-TiO_2 photocatalyst under visible-light irradiation. Reproduced from ref. 101. Copyright 2016, ACS.

improving carrier generation in AgBr. Eventually, AgBr plays the role of not only a visible-light photocatalyst but also an oxidation inhibitor of Ag clusters, while the Ag cluster with the LSPR effect acts as a visible light-driven amplifier for the local electric field. In addition, the built-in electric field could also be established by other methods, such as ferroelectric materials.[102]

In fact, Cushing *et al.*[103] summarized that there were three types of surface plasmon energy transfer mechanisms in metal/semiconductor systems due to the LSPR effect (shown in Fig. 8), which included the direct electron transfer (DET), also known as hot electron injection, the local electromagnetic field enhancement (LEMFE) and the plasma induced resonance energy transfer (PIRET). Each of these mechanisms is largely influenced by and functions through the electromagnetic field.

In DET, hot electrons can be promptly injected into the conduction band of the semiconductor accompanied by movement of chemical energy, and then transferred to the reaction substrate; alternatively, the hot electrons can directly react with reactants in contact with the metal NPs. In LEMFE, the absorbed solar energy is converted into electromagnetic energy *via* the oscillation of plasma. Distinguishingly, the enhanced electromagnetic field is confined within a few nanometers of the semiconductor surface. This is not the case for the normal, non-enhanced fields, which produce carriers too far below the semiconductor surface to contribute to photocatalysis due to the high recombination rate.[104] However PIRET is a non-radiation mechanism, which can be regarded as the energy of surface plasma resonance transferred from metal NPs to the semiconductor through the electromagnetic field or dipole interaction. To verify the PIRET mechanism, Torimoto *et al.*[105] wrapped SiO_2 on a Au/CdS composite photocatalyst, in which the SiO_2 insulating layer isolates the charge transfer channel between Au and CdS. In this efficient catalyst, the locally enhanced electric field is produced by photoexcitation of LSPR of Au NPs. The results showed that photocatalytic activity of CdS was greatly dependent on the distance between CdS and Au particles, and the range of energy dissipation is related to the diameter of the Au sphere. This non-contact energy transfer mechanism makes LSPR much more unique than any other photocatalysis modification method.

So far, there has been a continuous debate on these three mechanisms because of many arguments caused by distinct results from different researchers. For example, it was claimed that DET was beneficial to provide an effective electron transfer channel and there was no charge balance problem to be considered in this scheme.[103] However in the very beginning, DET was once considered to be impossible. It was deduced that since LSPR produced carriers with only a short lifetime ($\sim 10^{-12}$ s) as the excited hot-state, the activated adsorbate molecules that obtain electrons from the metal surface might also be quenched quickly.[106] On the opposite side, Brus[107] pointed out that the time of energy dissipation in DET was incorrectly evaluated. This is because energetic electrons, after being injected into the LUMO of the adsorbed molecules, can lead to the weakening and elongation of the original chemical bonds. The subsequent decay of generated transient anions with reduced energy and the reverse electron transfer to metal NPs can convert the energy into the molecular vibration. The average time required to dissipate this vibrational energy should be in the order of picoseconds ($\sim 10^{-9}$ s). Therefore, these typical chemical reactions are possible to occur if the energy adsorbed is sufficient to overcome the potential barrier that prevents the molecule decomposition.[33] In fact, in 2008, the direct photocatalytic reaction of metal NPs was experimentally observed.[108] Here, gold particles supported on ZrO_2 powders were prepared purposefully because the band gap of ZrO_2 is circa 5.0 eV, which are much larger than the energies of the photons of visible light (less than 3.0 eV). Thus, it is impossible for the gold NPs to reduce the band gaps of ZrO_2 enough for visible light photons to be absorbed and excite electrons in ZrO_2. Therefore, the visible-photocatalytic activity observed consequently confirms the photocatalytic ability of LSPR-produced energetic electrons.

As another example, it was reported that both DET and PIRET mechanisms exist in the core–shell structure of Au@Cu_2O[109] and Ag@Cu_2O.[110] However, due to the mutual constraints, the photocatalytic performance was not significantly enhanced especially when the two mechanisms were strongly overlapped.[4] Fig. 9 shows that with a relatively thin Cu_2O shell, the contributions of DET and PIRET strongly coincide and the resonance peak of LSPR is nearly at the Cu_2O

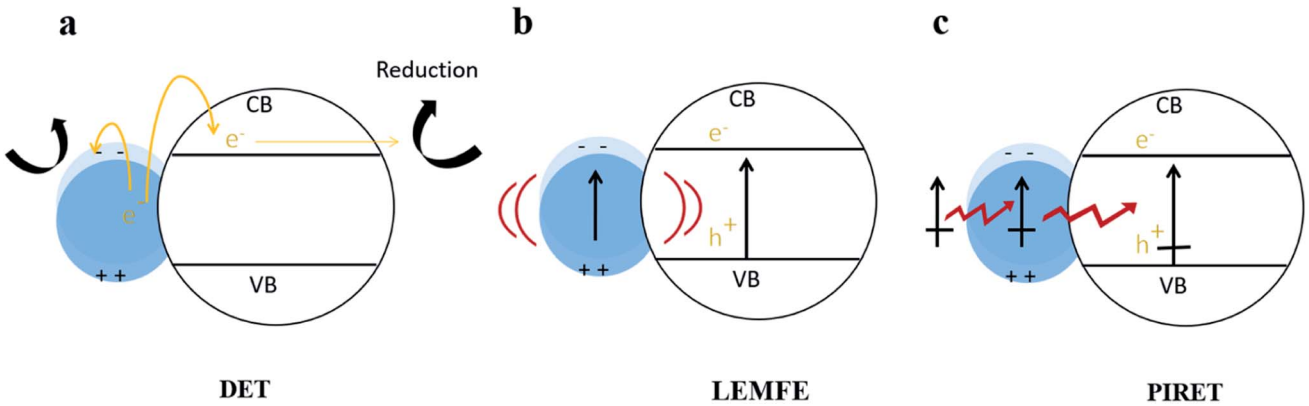

Fig. 8 Energy transfer mechanism in metal/semiconductor structures. Reprinted from ref. 103. Copyright 2012, ACS.

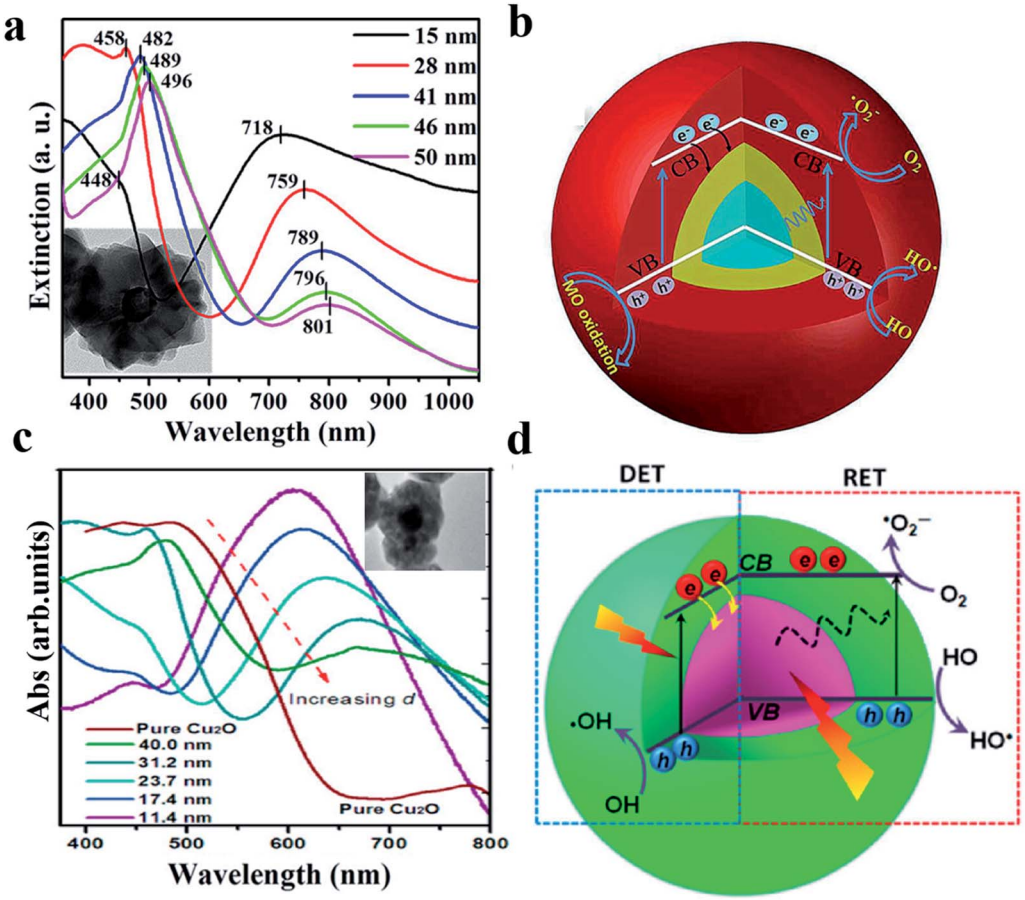

Fig. 9 (a) TEM and absorption spectra of the Au@Cu_2O core–shell NPs with various shell thicknesses. (b) Schematic illustration of the generation and transfer of electron–hole pairs in Au@Cu_2O core–shell NPs under visible-light irradiation. Reprinted from ref. 109. Copyright 2016, ACS. (c) TEM and absorption spectra of the Ag@Cu_2O core–shell NPs with various shell thicknesses. (d) Schematic architecture of simultaneous DET and PIRET in Ag@Cu_2O core–shell NPs. Reprinted from ref. 110. Copyright 2012, ACS.

absorption edge; however when the shell becomes thicker, the effects of DET and PIRET are gradually separated, resulting in the red shift of the resonance peak.

The above evidence of review shows that it is worth investigating deep into the energy transfer mechanism of LSPR-assisted catalysts and the specific interaction of DET, LEMF and PIRET in various scenarios. Thus, the feature of the electromagnetic field distribution is necessary to be specified. However, this fast transfer process makes it challenging to measure directly in time-resolved experiments. The existing experimental approaches to detect the charge transfer include XPS[111,112] and IR/Raman spectroscopy.[97,113,114] Besides, photocurrent can also reflect the overall photoelectric properties from a macro perspective.

Since the electromagnetic field distribution on the surface of particles can't be easily obtained at the nanometer scale, many scholars turned to use electromagnetic calculation methods, the essence of which is the Maxwell equations. The two most general ones are the analytical method and the numerical method. Before the maturity of the numerical calculation method, the analytical method is widely used but is not universal. For example, Mie scattering theory is the most basic algorithm for particle scattering, which is only suitable for small spherical particles.[115,116] The numerical calculation method can be divided into the frequency domain (such as the finite element method and discrete dipole approximation method) and the time domain (such as the finite difference time domain method). The frequency domain method has been developed earlier and is more mature at present, but its computational efficiency for some problems is lower than that of the time domain method.[117]

2.3 Heating effect

It has been reported that the local heating effect on the surface of metal NPs may lead to many special nanoscale phenomena.[118,119] Due to the photothermal effect, the excited electrons will return to the ground state in the form of releasing heat energy, causing the surface temperature of metal NPs to increase.

The increase of temperature has three effects on photocatalytic reactions:[120] first, speeding up the reaction rate. Before the whole photocatalytic reaction reaches the equilibrium, the augmented temperature is advantageous in increasing the

reaction rate. The influence could be more apparent for intermediate steps with a relatively slow reaction velocity. Second, increasing the carrier concentration of the catalyst. Because the carrier concentration increases with the increase of temperature, the introduction of a thermal field into the semiconductor can also help generate electron–hole pairs. It has been reported that under the synergistic effect of ultraviolet light and the thermal field, the photo excitation and thermal excitation could act on the conduction band electrons at the same time.[34] Li *et al.*[121] studied the normalized photoconductivity response in a CO_2 atmosphere at room temperature and 120 °C, respectively, and found that all TiO_2 samples with different oxygen vacancy contents showed higher photoconductivity at 120 °C. According to the decay curve of photoconductivity, Li concluded that the accelerated decay might be resulting from the improved charge-involved surface reaction. Therefore, it was speculated that the increase of temperature was beneficial to improve the transfer of electrons from the bulk to the surface and the concentration of surface carriers, thus adding the probability of reduction of CO_2. Third, increasing the light absorption of the catalyst. The intrinsic optical absorption of semiconductor is an indirect transition process, which needs to absorb or emit phonons to conserve the momentum of the transition. Hartland *et al.*[122] studied the basic optical properties of metal NPs which include the dynamic behavior after photon absorption. The results showed that the introduction of the thermal field intensified the lattice vibration in TiO_2 microcrystals and increased the quantity of phonons in the system. It was observed that the lattice temperature increased in a few picoseconds.[4] In this situation, the probability of phonon absorption and emission of conduction band electrons increased, which facilitated both the probability of indirect transition between bands and the light absorption efficiency significantly.

From the view of reaction dynamics, the reaction kinetic constant for the photo-thermal catalysis is generally larger than the values of the sole phenomenon, either the photocatalysis or the thermal catalytic kinetic constant.[123] The reasons for this phenomenon are summarized as follows: on the one hand, heat affects the molecular adsorption on the catalyst surface. Fu *et al.*[124] studied the photocatalytic degradation of ethylene in the temperature range of 30–110 °C. The results showed that the increase of the reaction temperature reduced the adsorption of water on the catalyst, which could provide more active sites for the ethylene reaction, thus improving the catalytic activity. Lin *et al.*[125] prepared oxidized ethylene with N-doped TiO_2. The kinetic analysis showed that water and ethylene would compete for the same active sites. The desorption of water during the heating process provided more reactive sites. On the other hand, thermal energy activates the lattice oxygen. Li's research group pointed out that the enhancement of photothermal catalytic activity was mainly ascribed to the active surface lattice oxygen.[126–128] It was found that the activity and content of lattice oxygen could be improved by increasing the temperature, resulting in the promotion of the lattice oxygen exchange and the increase of the adsorption rate of the organic substance at the solid–gas interface.

Li *et al.*[123] also proved that the photocatalytic efficiency could be markedly improved with the increase of temperature from the experimental view, as shown in Fig. 10. For the TiO_2 photocatalyst, when the temperature is increased from room temperature to 343 K, the degradation rate and mineralization rate of acetaldehyde increased by 2.7 times and 1.4 times, respectively. For WO_3 and ZnO photocatalysts, the mineralization rate of acetaldehyde at 333 K was 1.8 and 1.2 times higher than that at room temperature, respectively. In order to reveal the reasons for the improvement, Li changed the ambient humidity, the specific surface area and particle size of TiO_2. It was found that at different humidities, the degradation curve was approximately unchanged. Therefore, the temperature was not regarded to be conducive to the desorption of water on the surface and the exposing of active sites to adsorb the products. On the contrary, the experimental results showed that the samples with larger ratio of the surface to the volume gave a larger mineralization rate. This is because a larger ratio of the surface to the volume leads to a higher lattice oxygen content that can participate in the reaction. As a consequence, it is inferred that the surface lattice oxygen is the main reason for the improvement of photothermal catalytic oxidation activity in this research, as shown in Fig. 10f.

In comparison, the plasma nanostructure is more effective than most the other methods in converting the incident light into heat. Since solar energy can be converted into both chemical energy and heat, it is considered to be an effective strategy that the photocatalysis and thermal reaction are carried out simultaneously in the system.[129] The conversion of solar energy into photo-thermal-chemical energy is the research focus of the new generation photocatalysis.[130]

The existence of LSPR can improve the catalytic efficiency through the thermal confinement effect in the nano volume. However in principle, it is difficult to locate the heat producing region on the nanometer scale using traditional methods, making the plasma mediated heating unique to be utilized. The experiments by Ye *et al.*[131] showed that group VIII metals (Ru, Rh, Ni, Co, and Pt) could also produce the LSPR effect, which resulted in the increase of the surface temperature to 200 °C in 1 min. Therefore, the use of LSPR as the nano heat source to improve the chemical reaction rate and replace other additional energy sources has promising research prospect.

However, it is extremely difficult to directly detect the local temperature in the range of the nanometer size. Fortunately, numerical simulation has made an important contribution to the study of the surface temperature of NPs. Although the source of heat is not uniform, the steady-state temperature distribution of photothermally heated NPs can still be assumed to be uniform due to the ultrafast thermal equilibrium within the plasma.[132] By coupling Maxwell's equations with thermal diffusion equations, the steady-state temperature of plasmonic NPs can be obtained based on the numerical simulation.[133,134]

Nevertheless, some scholars argued that the high temperature caused by the photothermal effect might cause fundamental changes in the particle structure. For example, the team of Wei[133] demonstrated that the SPR-induced surface temperature of Ag–SiO_2 could be increased to above 230 °C under the irradiation of 2.0 W cm^{-2}, which was high enough to dissociate

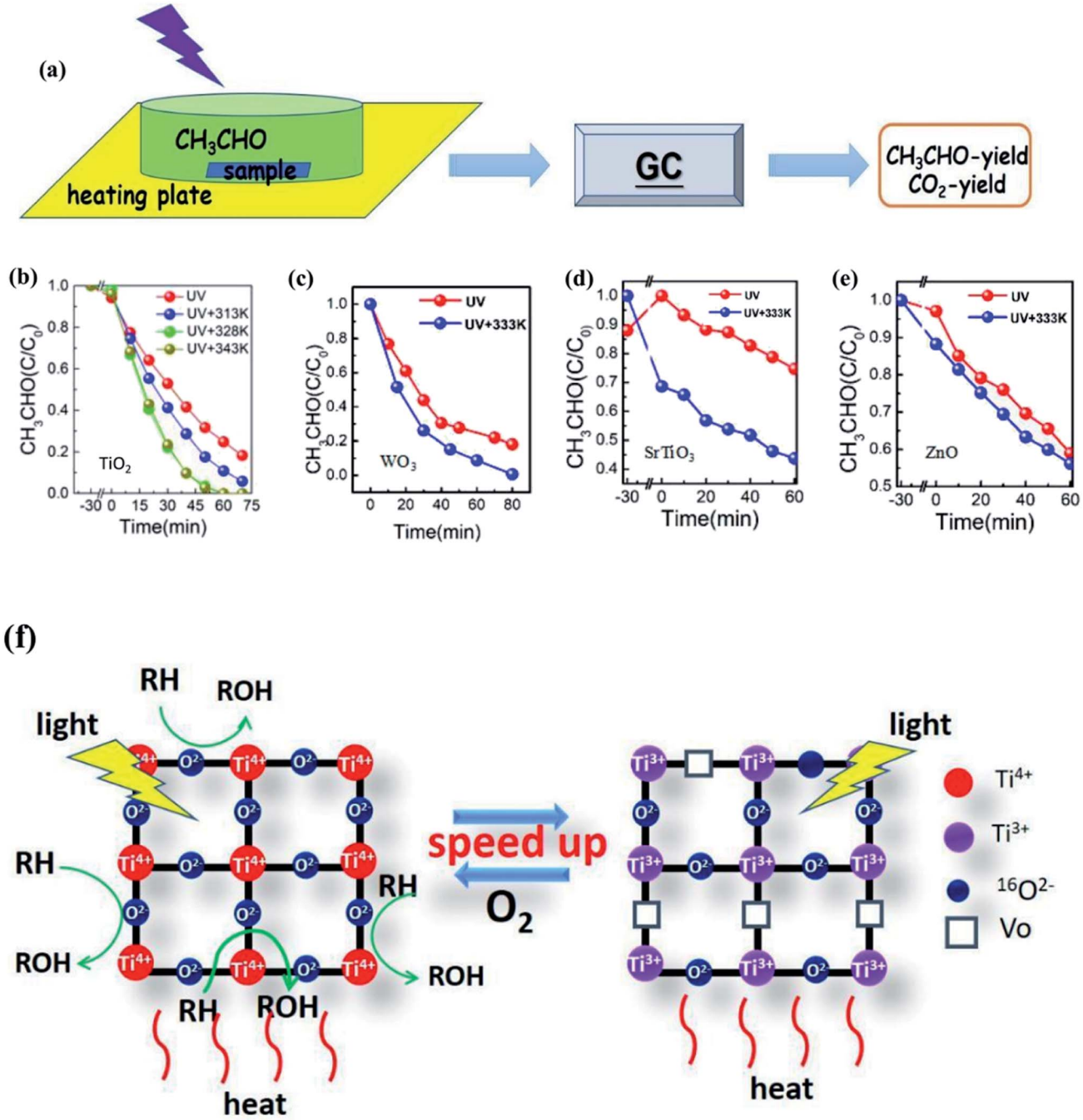

Fig. 10 (a) Experimental diagram of photo(thermal)catalytic degradation of CH_3CHO. (b)–(e) Photo(thermal)catalytic degradation rate of CH_3CHO. (f) Mechanism diagram of surface lattice oxygen of TiO_2 participating in the photothermal catalytic oxidation reaction. Reprinted from ref. 123.

the chemical bond. Some studies have also shown that the photothermal heating induced by LSPR could even melt and remodel Au NPs by using a high-power laser.[30,134] Therefore, many follow-up studies are still needed for the reasonable utilization of the LSPR thermal effect. Particularly, when analyzing the fracture and formation of the chemical bond and the reaction potential energy, the distribution of the nano-scale heat sources remains a crucial parameter that needs to be specified.

At present, the optical field and electromagnetic field based on numerical simulation are quantitatively studied. In fact, the temperature field also plays an important role in the photocatalytic system, which is worthy of more extensive and in-depth research. It should be emphasized that the optical, electrical, magnetic and thermal physical fields do not exist alone, but interact with each other in the photocatalytic system. Unfortunately, up to now, there is no comprehensive research on these four coupling physical fields. Instead, most researchers only

focus on one or two physical fields, such as the photoelectric effect, photothermal effect, *etc.*

3 Numerical solution of the photocatalytic physical field

With the continuous progress of computer technology, more and more researchers simulate the distribution of the physical fields in nanostructures by computational methods, such as the time domain finite difference method (FDTD), finite element method (FEM), and discrete dipole approximation method (DDA).

3.1 FDTD

Among the above calculation methods, FDTD is a mature numerical algorithm in the time domain, which can get the dynamic electromagnetic field characteristics directly. The core idea is to solve the differential equation by using the step difference of space and time, mesh the complex optical structure, and give the finite difference equation of time variable at each grid node. By setting the corresponding boundary conditions, the discrete time domain Maxwell degree of rotation equation is transformed into the display difference equation.[117,135] FDTD can also visualize the time evolution of the electromagnetic field. However, it is important to note that this method also has some disadvantages in application. For example, it is usually used to simulate structures with the given initial conditions and specific parameters. In the recent research on photocatalysis, the typical software based on the FDTD method is the Lumerical series. Also, the combination of Lumerical FDTD and the DEVICE simulator can realize the simulation of the photoelectric and thermal coupling field.

At present, many scholars have studied the optical absorption of plasma nanomaterials by Lumerical FDTD. Peng[26] studied the cubic column Al NPs, and analyzed the far-field extinction coefficient at different transverse and vertical ratios. Meanwhile, Liu[136] did similar simulation work and reported that LSPR had prominent wavelength selectivity for different metal NPs. It was found that the LSPR enhancement efficiency was not only closely related to the material, shape and size of metal NPs, but also to the particle spacing and aggregation morphology. Therefore, many scholars also considered the influence of different array forms. For example, Yu[137] from Nanjing University simulated the reflection spectrum of Na nanoarrays with different periods. In addition, Luan[138] established the Ag NP plasma resonance model by using East FDTD software. The surface plasmon resonance characteristics of the double spherical structure and triangular structure of Ag NPs were analyzed, and the influence of the particle size on the resonance absorption peak and transmission in the spherical array structure was discussed. These studies effectively solve the problem of predetermining the shape, the size, the interval distance and the period of metal NPs when designing LSPR assisted catalysts. Typically, Tira *et al.*[139] combined FDTD simulations with experiments to analyze the electromagnetic far-field and optical properties of Au NPs organized in chain-like structures (Fig. 11). As a result, an empirical formula to predict the position of collective LSPR as a function of the number of particles in the chain was developed, which offered useful design rules for the following LSPR-based applications.

In terms of electromagnetic field simulations, in order to further examine the interaction between metal NPs under the LEMFE effect, Christopher *et al.*[140] calculated the electric field intensity distribution around single and two Ag nanocubes by the FDTD method, respectively. According to their results, due to the LSPR excitation of a single cubic Ag NP, the intensity of surface electric fields is 10^3 times larger than the field intensity of the incoming photon flux. Interestingly, two Ag NPs separated in a narrow space could enhance the field intensity by 10^6 times.[141] Hou *et al.*[104] performed similar FDTD numerical

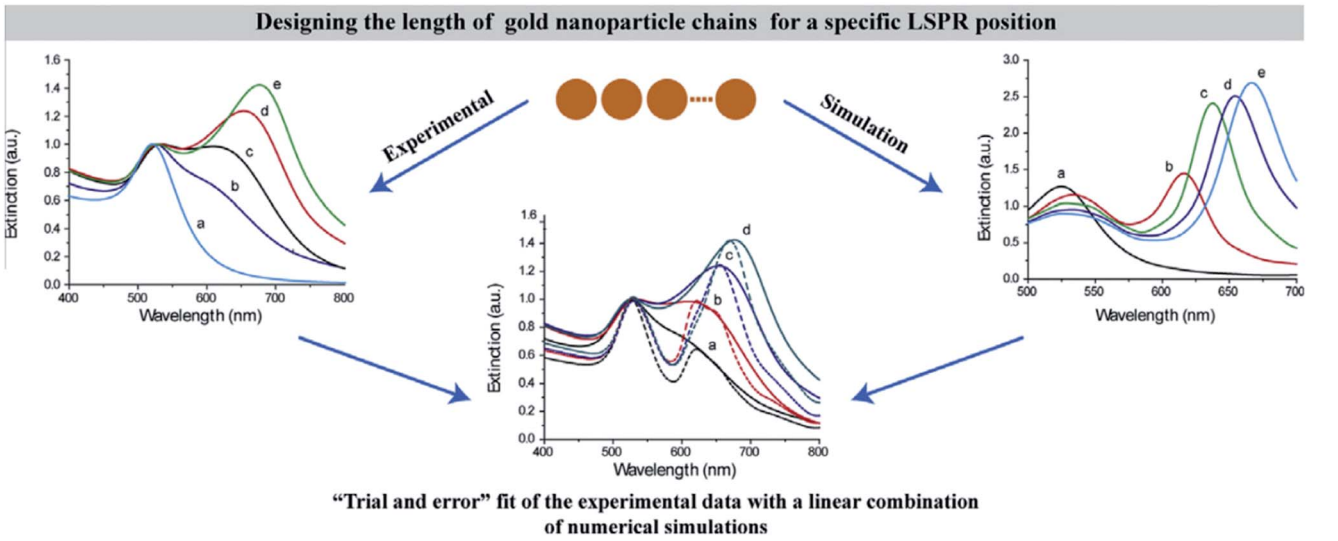

Fig. 11 Predesigning the length of gold NP chains for a specific LSPR position based on experimental data with a linear combination of numerical simulations.[139] Copyright 2014 Elsevier.

simulations of Au NPs/TiO_2 composites, as shown in Fig. 12. Local "hot spots" can be seen in regions between nearly touching Au NPs shown in Fig. 12d, which shows a cross-sectional plot of the electric fields in one of these hot spot regions. Since the photo absorption and hence the electron–hole pair generation rate is 1000 times higher than that of the normal incident light, and the enhanced field is confined within a few nanometers of the TiO_2 surface, most induced carriers efficiently diffuse to the surface so as to contribute to the catalytic reaction. This is not the case for the normal, since in non-enhanced fields, electron–hole pairs are usually produced distant from the TiO_2 surface. Based on the results of the FDTD electromagnetic simulations, Hou further calculated the expected photocatalytic enhancement due to LSPR. The obtained enhancement factor is consistent with the experimental observation. These simulation studies provide a feasible solution to further clarify the mechanism of the charge separation and energy transfer based on the electromagnetic field.

Additionally, FDTD could be well integrated with other calculation methods, typically density functional theory (DFT). Density functional theory, founded on quantum mechanics, is now widely used to quantitatively calculate the energy potential and the charge density distribution. In our previous work,[142] the DFT model was established to investigate the micro mechanism of CO_2 adsorption and the conversion of CO_2 to the $HCOO^*$ group in the Au–TiO_2 photocatalytic system. We simulated the CO_2 adsorption bonding in 6 configurations and obtained the adsorption energy, so as to figure out the way that CO_2 is converted into the $HCOO^*$ group in the step reaction. On this basis, by using FDTD simulations and DFT calculations, Guo systematically investigated the generation and modulation mechanism of the LSPR effect in Cu/TiO_2 nanospheres.[143] In Guo's study, the electrostatic potential and interfacial properties of the Cu/TiO_2 hetero-structure were calculated by DFT to analyze the impact of Cu NPs' LSPR effect on photocatalytic performance of TiO_2. However the optical resonance wavelength and electric field intensity were achieved from FDTD simulations to reflect the photocatalytic enhancement. This combination of FDTD and DFT methods is further effective to analyze the intrinsic mechanism of LSPR.

3.2 FEM

FEM is based on the basic strategy of discrete approximation, that is, a combination of many simple functions is used to approach the complex original function. In the recent research on photocatalysis, COMSOL is the typical software based on this method. COMSOL multiphysics software can realize any multiple physical field direct coupling analysis by solving the partial differential equation or equation system consisting of multiple fields.

In aspect of the simulation of optical properties, Liu[144] deduced the range of visible light resonance of TiO_2, Au/TiO_2, Ag/TiO_2 and other NPs based on COMSOL, which was beneficial to study the means of modulating LSPR to enhance the optical absorption. In addition, FEM can realize the coupling analysis of any temperature related physical field. Zhang *et al.*[145] from

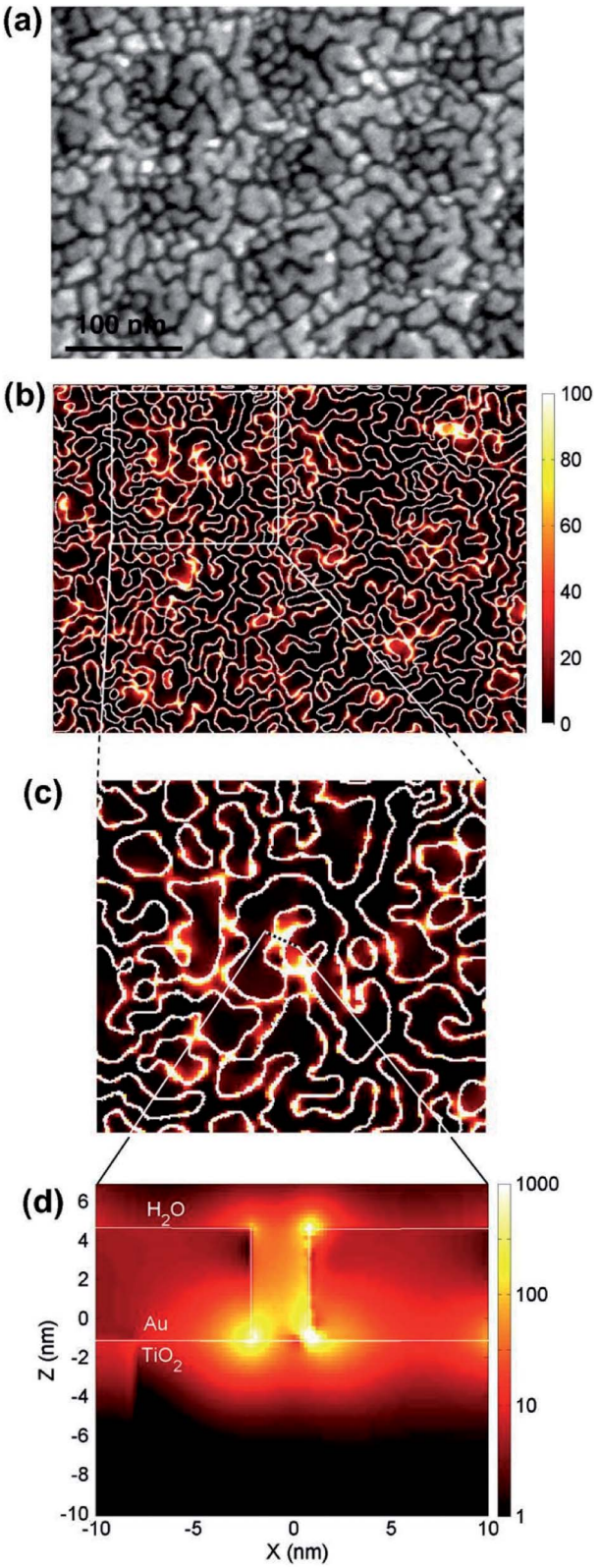

Fig. 12 (a) SEM image of a 5 nm thick Au island film deposited on anodic TiO_2. (b–d) Electric field intensities calculated at the interface of Au–TiO_2 using the FDTD method. Reprinted from ref. 104. Copyright 2011 Elsevier.

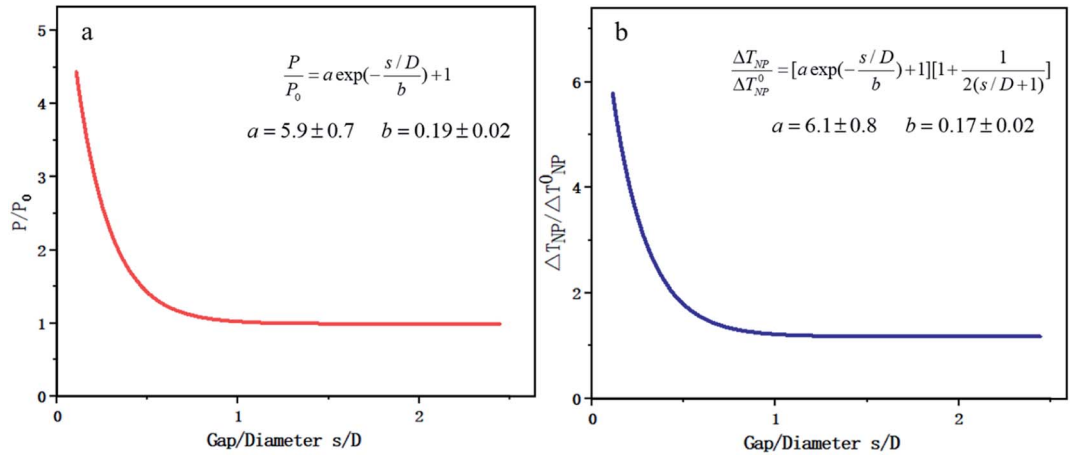

Fig. 13 Plasmon coupling of double Au NPs based on COMSOL. (a) Scaling law of light absorption power and relative particle spacing. (b) Scaling law of steady state temperature and relative particle spacing. Reproduced from ref. 145.

Zhejiang University used COMSOL to establish a universal scale equation depicting the relation between the photo-absorption/temperature and distance of two NPs. The objective was to make a practical equidistant excitation element ruler. It was found that the interaction effect between two metal NPs came from two aspects: on one hand the Coulomb coupling between the NPs enhanced the absorption of incident light, and on the other hand the accumulation of temperature made the heating effect more significant, as shown in Fig. 13. Zhang's research also provides some essential conclusions that key factors, such as the diameter of Au NPs and the gap between two NPs, may significantly help adjust the coupling physical fields.

Zhang's research considered the optical, electric, magnetic and thermal fields at the same time. However, the research is still restrained to the interaction between only two Au NPs. Therefore, it is worth combining multiple particles in the simulation and exploring the multi-physical fields under various temperature conditions.

Furthermore, Chen *et al.*[30] filled the investigation gap in the transient temperature behavior of a nanoscale plasmonic gold system during an ultra-fast photothermal process based on FEM shown in Fig. 14. A heat transfer model was constructed to analyze the temporal and spatial variation of temperature. The model shows that the temperature of the Au NPs can be increased from room temperature to more than 795 K in just a few nanoseconds with low light luminance, owing to enhanced light absorption through LSPR. Chen pointed out that such quantitative prediction of temperature change, which is otherwise formidable to measure experimentally, can serve as an excellent guideline for designing LSPR-based devices.

3.3 DDA

In the last few decades, FDTD and FEM have been the two most commonly used methods to simulate the photocatalysis phenomenon. Besides, DDA is another method to calculate the scattering electromagnetic wave of an object, which uses a large number of dipole arrays to simulate continuous objects. The properties of the electromagnetic waves are obtained by solving the polarization of dipoles under the incident electromagnetic

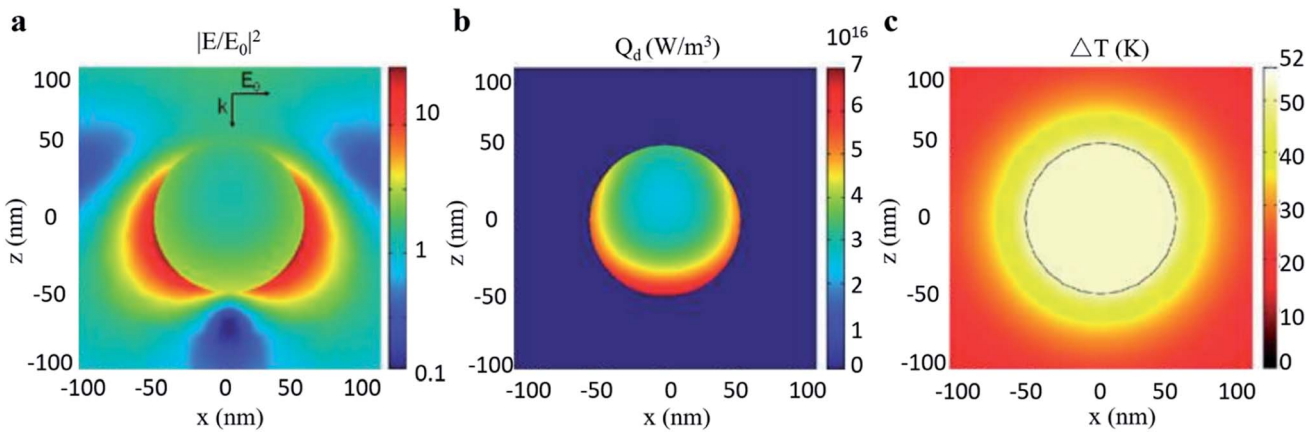

Fig. 14 Photothermal effect of a gold sphere with 50 nm radius in water. (a) Electric field intensity normalized to the incident field. (b) Heat power volume density Q_d. (c) Steady-state temperature increase due to 530 nm light excitation. Reprinted from ref [30]. Copyright 2012 American Chemical Society.

Table 4 Mean electric field enhancement factor values of Ag–Fe_3O_4 calculated using DDA[150]

		Particle size (nm)					
Target	Wavelength	3.5–13	7–13	10–13	13–13	16–13	20–13
Ag–Fe_3O_4	775 nm	1.10	1.20	1.35	1.56	1.81	2.18
	413 nm	1.11	1.40	2.06	3.19	4.92	7.83
Single Ag	775 nm	1.01	1.08	1.18	1.31	1.46	1.67
	413 nm	1.10	2.04	3.84	6.57	10.1	15.06

wave. In essence, DDA is a discrete expression of the integral form of the electromagnetic scattering formula.[146] DDSCAT is the typical software based on this method, which is a software package written by using the FORTRAN program and runs under the Linux system. For example, Shi *et al.*[147] from Jilin University used DDSCAT.5a10 to study the optical characteristics of different sizes of spherical, ellipsoidal, triangular prism and cylindrical Ag NPs. DDSCAT is suitable for isotropic, axisymmetric or non spherical particles with other symmetrical surfaces, resulting in relatively faster calculations compared to other software.[147–149]

Furthermore, Wang *et al.*[150] studied the electric field enhancement effect of Au–Fe_3O_4 and Ag–Fe_3O_4 based on DDA, as shown in Table 4. The results showed that when the polarization direction of the incident light was parallel to the inter particle axis and the incident light wavelength was equal to or greater than the LSPR wavelength, the absorption efficiency of the dimer and the electric field enhancement factor increased with the increase of the particle size, although the red shift of the LSPR wavelength was not apparent. However, except for the size factor, parametric study including the effect of the shape and spacing needs to be further investigated.

In the research of the multifield coupling mechanism, He *et al.*[151] studied the absorption spectra and the enhancement of the electric field in and near noble metal nanospheres (Au, Ag and Cu) based on DDA, which is proven to be fairly sensitive to the temperature, as shown in Fig. 15. The optical absorption peak and electric field enhancement within and near the NPs can all be changed by the temperature. In addition, the LSPR effect of Cu NPs may even be suppressed at a temperature of 700 K. These results provide new insights for understanding and improving the application performance of LSPR from the perspective of temperature control.

3.4 Advantages

According to the above review of the state-of-the-art literature on the physical fields of the LSPR assisted photocatalytic system, it is evident that the accurate predesign and difficult measurement of coupling fields are the current bottlenecks that restrain the application of LSPR assisted photocatalysis. Fortunately, the numerical simulation method has the following advantages that may provide potential solutions to these bottleneck problems:

Firstly, it is convenient to carry out comparisons based on the variable-controlling method. At present, many scholars have carried out experiments on one or several specific photocatalytic materials, but the conclusion is not universal. For example, Zhao[55] prepared four kinds of Al/TiO_2 composite photocatalysts with different TiO_2 contents. The photocatalytic performance

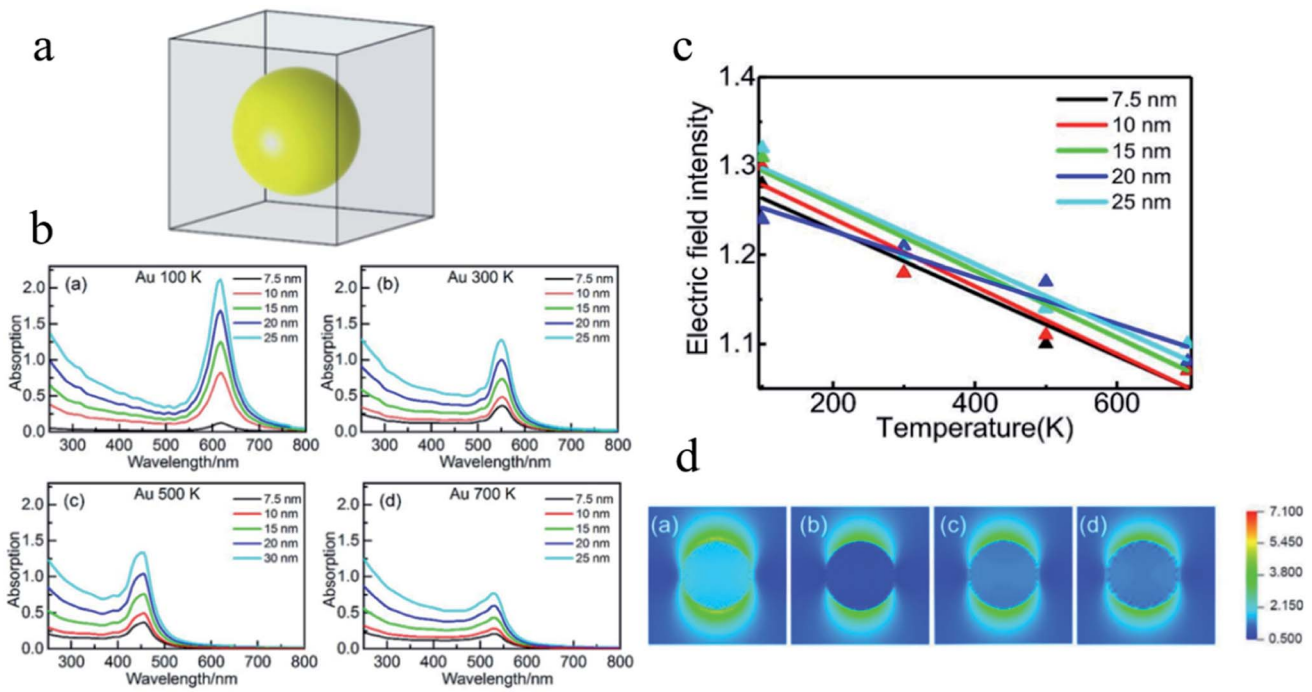

Fig. 15 (a) Structural model for DDA simulation. (b) Absorption efficiency *versus* the wavelength of Au NPs with different diameters at different temperatures. (c) Linear fitting of the averaged electric field intensity within the Au NPs at different temperatures. (d) Distribution of electric field intensity of Au NPs with a diameter of 7.5 nm at different temperatures. Reprinted from ref [151]. Copyright 2021 Springer.

for methylene blue degradation improved with the increase of the TiO_2 content, but the conclusion was not necessarily true if the catalyst materials or reaction conditions were changed.[152] In contrast, the numerical simulation can solve a large number of general problems and derive more control groups through predefined modules, which is more conducive to draw general conclusions.

Secondly, it provides a new way to design and precisely control metal composite nanostructures with excellent properties on demand. At the present stage, the preparation of most composite photocatalytic materials is complex. If noble metal particles are used for modification, the economic cost will also increase significantly. Zhang[153] used the FDTD simulation to establish the $Ag@SiO_2$ core–shell structure model, by which the parameters (Ag particle size, SiO_2 shell thickness and so on) under the LSPR resonance peak were calculated. Through the results of numerical simulation, Zhang predicted an improved photocatalytic system in advance to better guide the subsequent preparation work. Tira's[139] "trial and error" fit of the experimental data with a linear combination of FDTD simulations effectively realized predesigning the length of gold NP chains for a specific LSPR position. These research ideas are worthy of extensive reference.

Thirdly, the current numerical simulation software can basically realize the coupling calculations of multiple physical fields. Since the energy transfer mechanisms of metal NP induced catalysts are still debatable, visualization of physical fields is another advantage of numerical simulation, which can solve the micro-nano-scale problem that has difficulty in direct measurements by experiments. Therefore, it is convenient for scholars to understand and study the intrinsic mechanism.

In order to improve the photocatalytic efficiency, many important advances have been achieved by using the broadened visible light absorption, local electric field enhancement and thermal effect of LSPR. Nevertheless, a far-reaching investigation into the detailed and convincing mechanisms of how physical fields function in the photocatalytic reactions has not reached agreement among scholars.

This is because the LSPR effect involves synergistic enhancement of multifields. It is impossible to draw an accurate conclusion if only a single physical field is analyzed. For example, to study the path of electron charge transfer that was beneficially combined in a hybrid photo-thermal-catalytic reaction, Tan and coworkers reported a Au/TiO_2 catalyst for the photo-thermal-catalytic oxidation of ethanol.[154] Au/TiO_2 is a weak thermal catalyst, since under thermal catalytic conditions its catalytic performance only improves 5% compared with that of neat TiO_2. However, the results showed that Au/TiO_2 did show excellent photothermocatalytic activity under visible light and UV illumination (>175 °C). The catalytic performance was improved by more than 50% and 100% compared with that of neat TiO_2 under the above conditions, respectively. Based on the photo-thermal-catalytic results and detailed probing of postreaction surface carbon species, it is concluded that congruent roles of the photo and thermal catalysis contributed to the photo enhancement under UV irradiation, while under visible light irradiation plasmonic-mediated electron charge transfer from Au to TiO_2 played a significant role. It is noticed that the multifield coupling mechanism in LSPR is extremely complex due to many possibilities that need to be fully discussed under different situations. Furthermore, the integration of a LSPR-assisted catalyst with other photocatalysis-boosting techniques is another new trend according to the state-of-the art literature. The synergistic function mechanism behind these modification strategies, typically constructing a heterojunction[155] and loading a cocatalyst,[156] is also more sophisticated. Yang *et al.*[155] successfully fabricated the LSPR-assisted $CdIn_2S_4/W_{18}O_{49}$ Z-scheme heterojunction with a dual-channel

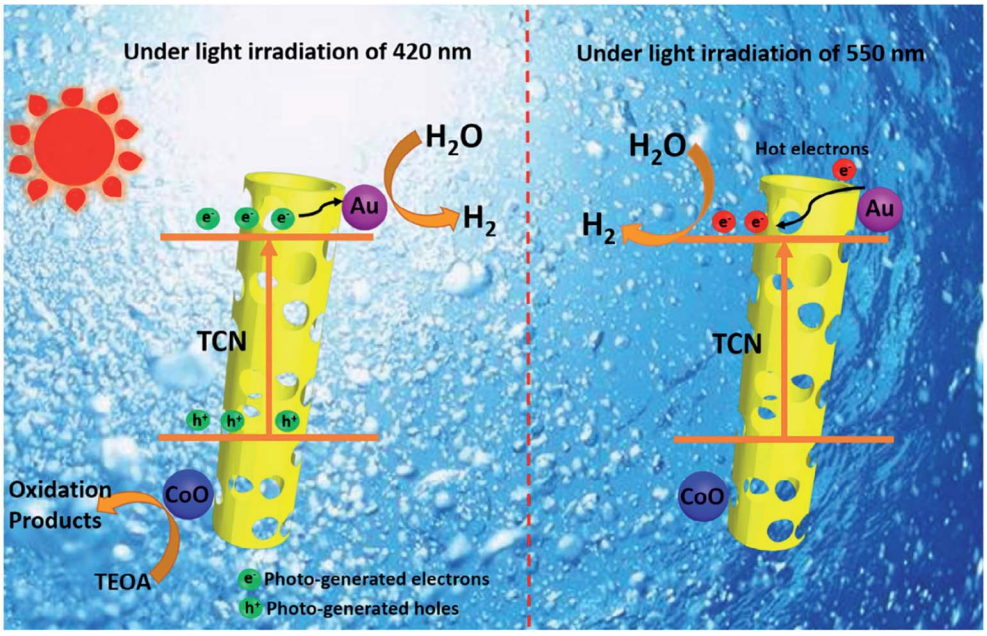

Fig. 16 Two distinct schemes of electron transfer over TCN/CoO/Au at 420 and 550 nm. Reprinted from ref [156]. Copyright 2020 Wiley.

charge transfer path, whose enhanced photocatalytic activity is ascribed to the synergistic effect of the heterojunction and LSPR effect. Specifically, the Z-scheme heterojunction and the LSPR-excited hot electron injection are the two beneficial pathways to promote charge transfer, while abundant oxygen vacancies that are associated with the LSPR effect exhibited efficient molecular oxygen activation activity. Liu *et al.*[156] integrated Au and CoO NPs with g-C_3N_4 hollow nanotubes to form a novel ternary hybrid, where Au served as a plasmonic antenna, hot electron donor, and reduction cocatalyst, and CoO acted as an oxidation cocatalyst. Noteworthily, the enhanced photocatalytic hydrogen evolution activity over a wide-light spectrum (420–650 nm) was believed to arise from two distinct electron transfer schemes at different wavelengths as shown in Fig. 16. To explain this complicated synergistic enhancement, multi-field decoupling is a basic necessity. Consequently, numerical simulations for decoupling of LSPR assisted photocatalysis is possible to be represented as an emerging direction for facilitating the development and application of visible light-driven photocatalysis.

4 Concluding remarks

In this paper, we systematically summarize the state-of-art advances of the photocatalytic efficiency improvement related to the optical, electrical, magnetic and thermal physical fields. Covering all the most widely-used modification methods, including heterojunctions, ion doping, dye sensitization and the introduced-LSPR effect, the photocatalytic enhancement principle is fundamentally illustrated and thoroughly compared. LSPR-assisted photocatalysis has apparent advantages because of the unique triple synergistic mechanism, while the current bottlenecks in it include the accurate predesign and difficult measurement of coupling fields. A knowledge gap remains in the fundamental revelation of how coupled physical fields function in the photocatalytic reactions. Thus, we focus on the potential of numerical simulations for examining the interaction of the multi-physical field. The conclusions, challenges and opportunities of the photocatalysis research are shown below:

(1) Notably, LSPR assisted photocatalysts possess three excellent advantages, that is, the broadened absorption spectrum, local electric field enhancement and the thermal effect, which largely promote the reaction efficiency based on multi physical fields. Thus, the LSPR effect is a noteworthy research direction for next generation photocatalysts, which puts forward strict requirements for the preparation of noble metal NPs with low cost, high efficiency and controllable modulation. Accurate predesign is indispensable to optimize the spectral characteristics and create a proper built-in field, since key parameters, like the particle size, shape, the gap between NPs and structure, directly affect the LSPR efficiency. Also, there is no general rule regarding the modification effect of LSPR-assisted photocatalysts yet. Although many scholars have carried out experimental research studies on LSPR-assisted photocatalysts, the conclusions are not universal and systematic due to the lack of unified standard systems. Moreover, the reaction parameters (such as the lamp source, pressure, material amount, *etc.*) are not universally given in different investigations, causing the difficulty for comparison and evaluation of the photocatalytic activity under the same criteria. Precisely designed LSPR-assisted nanostructures on demand and carrying out comparisons based on the variable-controlling method are the appealing directions for the numerical simulation methods in this field.

(2) Because of the micro-nano localization of the LSPR effect, it is difficult to measure the nano scale system directly, which leads to the debatable energy transfer mechanisms of metal NP induced catalysts to a certain extent. Visualization and calculation of coupling physical fields is another advantage of numerical simulations, which can help overcome the difficulties in experiments. FDTD, FEM and DDA, each of the three has its unique advantages in solving these bottleneck problems on the proper utilization of LSPR. Markedly, the optical absorption performance, electric field intensity distribution and temperature rise effect can all be achieved through the simulation methods. Integrated with other calculation methods like density functional theory, the simulation research is also further effective to analyze the intrinsic mechanism of LSPR and provide a theoretical reference for the efficiency enhancement.

(3) It must be noted that LSPR is actually a multifield synergistic effect, which indicates the impossibility of elucidating the reason of photo-thermal enhancement by investigation of a single physical field. Since the complex mechanism of the optical, electrical, magnetic and thermal fields triggered by the LSPR effect is still controversial, the interaction of the multi-fields is still worthy to be investigated due to the lack of principle interpretation for the photocatalyst activity enhancement. Also, the integration of the LSPR-assisted catalyst and other improvement techniques, typically constructing a heterojunction and loading the cocatalyst, is the new trend for photocatalysis. And the synergistic function mechanism behind these modification strategies is more sophisticated. Multifield decoupling of LSPR assisted photocatalysis by numerical simulations is promising to be focused on in the future. This is reasonable as the electromagnetic field distribution can be visualized, based on which the nano heat source within the photocatalysts can be quantitatively studied.

Conflicts of interest

There are no conflicts to declare.

Acknowledgements

The research was financially supported by the National Natural Science Foundation of China (No. 52076139).

References

1 X. Tan, M. Fang, J. Li, *et al.*, Adsorption of Eu(III) onto TiO_2: effect of pH, concentration, ionic strength and soil fulvic acid, *J. Hazard. Mater.*, 2009, **168**(1), 458–465.

2 S. G. Kumar and L. G. Devi, Review on Modified TiO_2 Photocatalysis under UV/Visible Light: Selected Results and Related Mechanisms on Interfacial Charge Carrier Transfer Dynamics, *J. Phys. Chem. A*, 2011, **115**(46), 13211–13241.

3 J. Wu, K. Chen, X. Tan, *et al.*, Core–shell CMNP@PDAP nanocomposites for simultaneous removal of chromium and arsenic, *Chem. Eng. J.*, 2018, S1385894718309288.

4 G. Y. Yao, Q. L. Liu and Z. Y. Zhao, Applications of Localized Surface Plasmon Resonance Effect in Photocatalysis, *Prog. Chem.*, 2019, **31**(4), 516–535.

5 A. Hagfeldt and M. Graetzel, Light-induced redox reactions in nanocrystalline systems, *Chem. Rev.*, 1995, **95**(1), 49–68.

6 L. Gao, *Study on quantum size effect of II–VI semiconductor nanomaterials*, Yanshan University, 2018.

7 Y. P. Yuan, L. W. Ruan, J. Barber, *et al.*, Hetero-nanostructured suspended photocatalysts for solar-to-fuel conversion, *Energy Environ. Sci.*, 2014, **7**(12), 3934–3951.

8 J. Peng, J. Shen, X. Yu, H. Tang, Zulfiqar and Q. Liu, Construction of LSPR-enhanced 0D/2D CdS/MoO_{3-x} S-scheme heterojunctions for visible-light-driven photocatalytic H_2 evolution, *Chin. J. Catal.*, 2021, **42**(1), 87–96.

9 O. A. Balitskii, Recent Energy Targeted Applications of LSPR Semiconductor Nanocrystals: a mini-Review, *Mater. Today Energy*, 2020, **20**, 100629.

10 S. Xie, H. Zhang, G. Liu, X. Wu, J. Lin, Q. Zhang and Y. Wang, Tunable localized surface plasmon resonances in MoO_{3-x}-TiO_2 nanocomposites with enhanced catalytic activity for CO_2 photoreduction under visible light, *Chin. J. Catal.*, 2020, **41**(7), 1125–1131.

11 H. Wang, J. Tao, J. Lu, D. Meng, Y. Li, Y. Zhao, J. Wang, J. Zhang, Y. Qin, W. Wang and J. Liang, Absorption enhancement of silicon via localized surface plasmons resonance in blue band, *Chin. J. Opt.*, 2020, **13**(6), 1362–1384.

12 M. A. Garcia, Surface plasmons in metallic nanoparticles: fundamentals and applications, *J. Phys. D: Appl. Phys.*, 2011, **44**(28), 283001.

13 J. Qiu and W. D. Wei, Surface Plasmon-Mediated Photothermal Chemistry, *J. Phys. Chem. C*, 2014, **118**(36), 20735–20749.

14 S. Cao, S. Zhang, T. Zhang, *et al.*, Metal-doped TiO_2 colloidal nanocrystals with broadly tunable plasmon resonance absorption, *J. Mater. Chem. C*, 2018, **10**, 1039.

15 H. T. Chou, W. H. Huang, T. M. Wu, *et al.*, LSPR effects of Au nanoparticles/ZnO nano-composite films, *Sens. Bio-Sens. Res*, 2017, **14**, 17–20.

16 A. Tanaka, K. Hashimoto and H. Kominami, A very simple method for the preparation of Au/TiO_2 plasmonic photocatalysts working under irradiation of visible light in the range of 600–700 nm, *Chem. Commun.*, 2017, **53**, 4759–4762.

17 H. Wang, Y. Wang, L. Guo, *et al.*, Solar-heating boosted catalytic reduction of CO_2 under full-solar spectrum, *Chin. J. Catal.*, 2020, **41**(1), 131–139.

18 X. Zheng, D. Zhang, Y. Gao, *et al.*, Synthesis and characterization of cubic Ag/TiO_2 nanocomposites for the photocatalytic degradation of methyl orange in aqueous solutions, *Inorg. Chem. Commun.*, 2019, **110**, 107589.

19 T. C. Dechakiatkrai and P. Sukon, Visible-Light-Induced Photocatalytic Degradation of PAH-Contaminated Soil and Their Pathways by Fe-Doped TiO_2 Nanocatalyst, *Water, Air, Soil Pollut.*, 2018, **229**(9), 291.

20 G. Y. Yao and Z. Y. Zhao, Unraveling the Role of Cuprous Oxide and Boosting Solar Energy Conversion via Interface Engineering in Cu/TiO_2 Plasmonic Photocatalyst, *J. Mater. Chem. C*, 2020, **8**, 8567–8578.

21 A. Podlipensky, A. Abdolvand, G. Seifert, *et al.*, Femtosecond laser assisted production of dichroitic 3D structures in composite glass containing Ag nanoparticles, *Appl. Phys. A: Mater. Sci. Process.*, 2005, **80**(8), 1647–1652.

22 T. Jin, *Fabrication, Characterization and Modulation of Nanoparticles in SiO_2 Implanted with Ni, Ag Ions*, Taiyuan University of Technology, 2014.

23 X. Yue, *Preparation of Au-based alloy nanoparticles and study on enhanced photocatalytic performance*, Shihezi University, 2020.

24 C. Lin, *Controllable Preparation of Au@SnO_2 Core–Shell Plasmonic Materials and Its Photocatalytic Performance*, Jiangsu University, 2020.

25 S. Link and M. A. El-Sayed, Shape and size dependence of radiative, non-radiative and photothermal properties of gold nanocrystals, *Int. Rev. Phys. Chem.*, 2000, **19**(3), 409–453.

26 H. Peng, C. Ge, J. Zhou, *et al.*, Simulation and analysis of the effect of Al nano-particle size on the characteristics of LSPR, *Optoelectronic Technology*, 2020, **40**(3), 176–179.

27 Z. Jiao, *Preparation, regulation and performance characterization of gold and alloy nanocrystals*, Shandong University, 2011.

28 Z. Pang, L. Wan, J. Huang, *et al.*, Study on the relationship between properties of localized surface plasmon resonance and surface shape parameter of metal nanoparticles, *Journal of Light Scattering*, 2014, **26**(3), 307–315.

29 Z. He, *Photocatalytic reduction of carbon dioxides by plasmonic silver-based composite photocatalyst under visible light irradiation*, Zhejiang University of Technology, 2014.

30 X. Chen, Y. Chen, M. Yan, *et al.*, Nanosecond Photothermal Effects in Plasmonic Nanostructures, *ACS Nano*, 2012, **6**(3), 2550–2557.

31 C. Fasciani, C. Alejo, M. Grenier, *et al.*, High-temperature organic reactions at room temperature using plasmon excitation: decomposition of dicumyl peroxide, *Organic Letters*, 2011, **13**(2), 204–207.

32 P. K. Jain, W. Qian and M. A. El-Sayed, Ultrafast cooling of photoexcited electrons in gold nanoparticle-thiolated DNA conjugates involves the dissociation of the gold-thiol bond, *J. Am. Chem. Soc.*, 2006, **128**(7), 2426–2433.

33 P. Christopher, H. Xin and S. Linic, Visible-light-enhanced catalytic oxidation reactions on plasmonic silver nanostructures, *Angew. Chem.*, 2011, **3**, 467.

34 C. Wei, C. Yu, K. Yang, *et al.*, Recent advances in VOCs and CO removal via photothermal synergistic catalysis, *Chin. J. Catal.*, 2021, **42**(7), 1078–1095.

35 J. Kong, C. Jiang, Z. Rui, *et al.*, Photothermocatalytic synergistic oxidation: an effective way to overcome the negative water effect on supported noble metal catalysts for VOCs oxidation, *Chem. Eng. J.*, 2020, **397**, 125485.

36 R. Lu, M. Mingyang, *et al.*, Novel photothermocatalytic synergetic effect leads to high catalytic activity and excellent durability of anatase TiO_2 nanosheets with dominant 001 facets for benzene abatement, *Appl. Catal., B*, 2016, **198**, 303–310.

37 X. Wang, D. Zeng and C. Xie, Temperature-dependent photothermocatalytic mineralization of gaseous benzene based on rutile TiO_2 nanorod array, *Mater. Lett.*, 2015, **139**(15), 336–339.

38 Y. Li, J. Huang, *et al.*, Photothermocatalytic Synergetic Effect Leads to High Efficient Detoxification of Benzene on TiO_2 and Pt/TiO_2 Nanocomposite, *ChemCatChem*, 2010, **2**(9), 1082–1087.

39 X. Fu, W. A. Zeltner and M. A. Anderson, The gas-phase photocatalytic mineralization of benzene on porous titania-based catalysts, *Appl. Catal., B*, 1995, **6**(3), 209–224.

40 J. Huang, *Preparation and photocatalytic performance of TiO_2 and Pt/TiO_2 nano composite photocatalyst based on thermocatalytic synergetic effect*, Wuhan University of Technology, 2010.

41 J. C. Kennedy III and A. K. Datye, Photothermal Heterogeneous Oxidation of Ethanol over Pt/TiO_2, *J. Catal.*, 1998, **179**(2), 375–389.

42 H. U. Chun, L. Y. Lin and H. U. Xue-Xiang, Morphology of metal nanoparticles photodeposited on TiO_2/silical gel and photothermal activity for destruction of ethylene, *J. Environ. Sci.*, 2006, **18**(1), 76–82.

43 X. Li, *Preparation and field responses of nanosized recombined multi-parametric functional oxides*, University of Science and Technology of China, 2016, vol. 1.

44 G. Baffou and R. Quidant, Nanoplasmonics for Chemistry, *Chem. Soc. Rev.*, 2014, **43**, 3898.

45 C. Tao, T. Fengxia, E. Jrg, *et al.*, Plasmon-Driven Modulation of Reaction Pathways of Individual Pt-Modified Au Nanorods, *Nano Lett.*, 2020, (5), 3326–3330.

46 X. Xie, *Research on sensing characteristics of nanoparticles based on FDTD simulation and application research*, Ji Mei University, 2019.

47 J. Zhong, *Research on plasmonic catalysis of gold nanoparticles and their composite structures*, Henan University, 2020.

48 S. Manrique-Bedoya, M. Abdul-Moqueet, P. Lopez, *et al.*, Multiphysics Modeling of Plasmonic Photothermal Heating Effects in Gold Nanoparticles and Nanoparticle Arrays, *J. Phys. Chem. C*, 2020, **124**, 17172–17182.

49 S. P. Tiwari, A. Kumar, K. Kumar, *et al.*, LSPR-mediated improved upconversion emission on randomly distributed gold nanoparticles array, *New J. Chem.*, 2020, **44**, 19672–19682.

50 X. Wang, Y. Wang, X. Yang, *et al.*, Numerical simulation on the LSPR-effective core-shell copper/graphene nanofluids, *Sol. Energy*, 2019, **181**, 439–451.

51 Z. A. Jian, B. Wl, B. Hl, *et al.*, Yolk–shell@TiO_2 composite particles with photocorrosion resistance for enhanced dye removal and hydrogen evolution, *Adv. Powder Technol.*, 2019, **30**(9), 1965–1975.

52 C. Yang, J. Qin, Z. Xue, *et al.*, Rational design of carbon-doped TiO_2 modified g-C_3N_4 via in situ heat treatment for drastically improved photocatalytic hydrogen with excellent photostability, *Nano Energy*, 2017, S2211285517305505.

53 J. Liu, X. Wei, W. Sun, *et al.*, Fabrication of S-scheme CdS-g-C_3N_4-graphene aerogel heterojunction for enhanced visible light driven photocatalysis, *Environ. Res.*, 2021, 111136.

54 H. Yang, A short review on heterojunction photocatalysts: carrier transfer behavior and photocatalytic mechanisms, *Mater. Res. Bull.*, 2021, **142**, 111406.

55 X. Zhao, Z. Lu, W. Ma, *et al.*, One-step fabrication of carbon decorated $CO_3O_4/BiVO_4$ p–n heterostructure for enhanced visible-light photocatalytic properties, *Chem. Phys. Lett.*, 2018, S0009261418304330.

56 M. N. Magaa, S. C. Díaz and R. Gomez, Improved photocatalytic oxidation of arsenic(III) with WO_3/TiO_2 nanomaterials synthesized by the sol–gel method, *J. Environ. Manage.*, 2021, (5528), 282.

57 Z. N. Kayani, H. Bashir, S. Riaz, *et al.*, Optical properties and antibacterial activity of V doped ZnO used in solar cells and biomedical applications, *Mater. Res. Bull.*, 2019, **115**, 121–129.

58 Y. Jia, W. Zhang and J. Yeon Do, ZScheme $SnFe_2O_4/\alpha$-Fe_2O_3 Micro-octahedron with Intimated Interface for Photocatalytic CO_2 Reduction, *Chem. Eng. J.*, 2020, **402**, 126193.

59 G. Cordeiro, I. Silva, T. Veríssimo, *et al.*, Photocatalytic properties of SnO_2/MoO_3 mixed oxides and their relation to the electronic properties and surface acidity, *J. Photochem. Photobiol., A*, 2021, **407**, 113035.

60 M. Liu, P. Li, S. Wang, *et al.*, Hierarchically porous hydrangea-like In_2S_3/In_2O_3 heterostructures for enhanced photocatalytic hydrogen evolution, *J. Colloid Interface Sci.*, 2021, **587**, 876–882.

61 J. Zhao, Z. Zhao, L. Ning, *et al.*, Visible-light-driven photocatalytic degradation of ciprofloxacin by a ternary $Mn_2O_3/Mn_3O_4/MnO_2$ valence state heterojunction, *Chem. Eng. J.*, 2018, S1385894718314128.

62 Y. Wang, H. Yang, X. Sun, *et al.*, Preparation and photocatalytic application of ternary n-$BaTiO_3$/Ag/p-AgBr heterostructured photocatalysts for dye degradation, *Mater. Res. Bull.*, 2020, **124**, 110754.

63 Y. Long, L. Li, L. Zhou, *et al.*, Fabrication of the AgI/BiOI/$BiPO_4$ multi-heterojunction with high photocatalytic activity – Science Direct, *Mater. Res. Bull.*, 2020, **126**, 110787.

64 D. Osorio-Rivera, G. Torres-Delgado, R. Castanedo-Pérez, *et al.*, $Cd_2SnO_4/CdS/Cu_2O$/Ag solar cell obtained by chemical techniques, *Mater. Res. Bull.*, 2019, **122**, 110669.

65 N. Thirugnanam, H. Song and Y. Wu, Photocatalytic degradation of Brilliant Green dye using CdSe quantum dots hybridized with graphene oxide under sunlight irradiation, *Chin. J. Catal.*, 2017, **38**(12), 2150–2159.

66 Z. Zhang, L. Bai, Z. J. Li, *et al.*, Review on constructed strategies of heterojunctional nanocomposites as efficient visible-light catalysts by modulating excited electrons with appropriate thermodynamic energy, *J. Mater. Chem. A*, 2019, **7**, 10879–10897.

67 R. T. Asahi, T. Morikawa, T. Ohwaki, *et al.*, Visible-Light Photocatalysis in Nitrogen-Doped Titanium Oxides, *Science*, 2001, **293**(5528), 269–271.

68 W. Yu, J. Zhang and T. Peng, New insight into the enhanced photocatalytic activity of N-, C- and S-doped ZnO photocatalysts, *Appl. Catal., B*, 2016, 220–227.

69 R. Zheng, G. Ying, J. Chen, *et al.*, Novel thermally stable phosphorus-doped TiO_2 photocatalyst synthesized by hydrolysis of $TiCl_4$ – ScienceDirect, *J. Mol. Catal. A: Chem.*, 2010, **319**(1–2), 46–51.

70 Y. Wei, X. Liu, L. Pan, *et al.*, Enhanced visible light photocatalytic degradation of methylene blue by F-doped TiO_2, *Appl. Surf. Sci.*, 2014, **319**(15), 107–112.

71 M. Wang, C. Wang, Y. Liu, *et al.*, Hybrid density functional theory description of non-metal doping in perovskite $BaTiO_3$ for visible-light photocatalysis, *J. Solid State Chem.*, 2019, **280**, 121018.

72 C. Balasanthiran, S. Jensen, C. S. Spanjers, *et al.*, Quantitative Attachment of Bimetal Combinations of Transition-Metal Ions to the Surface of TiO_2 Nanorods, *Langmuir*, 2018, **34**(19), 5422–5434.

73 F. Liu, L. Xu, Y. Xiu, *et al.*, Non-metallic element doped titanium dioxide, *Chemistry*, 2021, **84**(2), 108–119.

74 X. Zhou, *Synthesis and characterization of dye-sensitized TiO_2 photocatalyst*, Nort University of China, 2021.

75 M. R. Narayan, Review: dye sensitized solar cells based on natural photosensitizers, *Renewable Sustainable Energy Rev.*, 2011, **16**(1), 208–215.

76 C. Huang, Y. Lv, Q. Zhou, *et al.*, Visible photocatalytic activity and photoelectrochemical behavior of TiO_2 nanoparticles modified with metal porphyrins containing hydroxyl group, *Ceram. Int.*, 2014, **40**(5), 7093–7098.

77 J. A. Khan, M. Sayed, N. S. Shah, *et al.*, Synthesis of eosin modified TiO2 film with co-exposed {001 and {101 facets for photocatalytic degradation of para -aminobenzoic acid and solar H_2 production, *Renewable Sustainable Energy Rev.*, 2020, **265**, 118557.

78 T. Phongamwong, W. Donphai, P. Prasitchoke, *et al.*, Novel visible-light-sensitized Chl-Mg/P25 catalysts for photocatalytic degradation of rhodamine B, *Appl. Catal., B*, 2017, **207**, 326–334.

79 C. Diaz-Uribe, W. Vallejo, E. Romero, *et al.*, TiO_2 thin films sensitization with natural dyes extracted from Bactris guineensis for photocatalytic applications: experimental and DFT Study, *J. Saudi Chem. Soc.*, 2020, **24**(5), 407–416.

80 S. Meng, J. Ren and E. Kaxiras, Natural Dyes Adsorbed on TiO_2 Nanowire for Photovoltaic Applications: Enhanced Light Absorption and Ultrafast Electron Injection, *Nano Lett.*, 2008, **8**(10), 3266–3272.

81 Z. Zheng, *Development of plasmonic photocatalyst by site-selective loading of bimetallic nanoparticles of Au and Ag on titanium (IV) oxide*, Yangzhou University, 2020.

82 K. Jain Prashant, K. S. Lee, H. El-Sayed Ivan and A. El-Sayed Mostafa, Calculated absorption and scattering properties of gold nanoparticles of different size, shape, and composition: applications in biological imaging and biomedicine, *J. Phys. Chem. B*, 2006, **110**(14), 7238–7248.

83 R. Jiang, S. Cheng, L. Shao, *et al.*, Mass-Based Photothermal Comparison Among Gold Nanocrystals, PbS Nanocrystals, Organic Dyes, and Carbon Black, *J. Phys. Chem. C*, 2013, **117**(17), 8909.

84 D. Mortazavi, A. Z. Kouzani, A. Kaynak, *et al.*, Developing LSPR design guidelines, *Prog. Electromagn. Res.*, 2012, **126**, 203–235.

85 X. Wang, Y. Wang, X. Yang, *et al.*, Numerical simulation on the LSPR-effective core–shell copper/graphene nanofluids, *Sol. Energy*, 2019, **181**, 439–451.

86 L. H. Zhang, *et al.*, Preparation of core–shell Ag@CeO_2 nanocomposite by LSPR photothermal induced interface reaction, *Nanotechnology*, 2016, **27**(13), 135701.

87 M. Gao, Y. Song, Y. Liu, *et al.*, Controlled fabrication of Au@MnO_2 core/shell assembled nanosheets by localized surface plasmon resonance, *Appl. Surf. Sci.*, 2021, **537**, 147912.

88 Z. Liu, J. Ye, *et al.*, Highly controllable double Fano resonances in plasmonic metasurfaces, *Nanoscale*, 2016, **8**(40), 17665–17674.

89 K. Wu, T. Rindzevicius, M. S. Schmidt, *et al.*, Plasmon resonances of Ag capped Si nanopillars fabricated using mask-less lithography, *Opt. Express*, 2015, **23**(10), 12965–12978.

90 M. Shabaninezhad and G. Ramakrishna, Theoretical Investigation of Size, Shape and Aspect Ratio Effect on the LSPR Sensitivity of Hollow-Gold Nanoshells, *J. Chem. Phys.*, 2019, **150**(14), 144116.

91 H. H. Sun, H. S. Dong, J. Yun, *et al.*, SiO_2/TiO_2 Hollow Nanoparticles Decorated with Ag Nanoparticles: Enhanced Visible Light Absorption and Improved Light Scattering in Dye-Sensitized Solar Cells, *Chem.–Eur. J.*, 2014, **20**(15), 4439–4446.

92 B. Yu, F. Meng, T. Zhou, *et al.*, Construction of hollow TiO_2/CuS nanoboxes for boosting full-spectrum driven photocatalytic hydrogen evolution and environmental remediation, *Ceram. Int.*, 2020, **47**(7), 8849–8858.

93 M. Liu, *Modulating the absorption and near field properties of Au-TiO_2 nanohybrids for photocatalytic application*, Jiangsu University, 2020.

94 Y. Chen, Q. Wang, J. Kou, *et al.*, Efficient photocatalytic H_2 production realized by $Mn_xCd_{1-x}Se$ in situ heterojunction, *Nanotechnology*, 2021, **32**(36), 365602.

95 W. He, L. Liu, T. Ma, *et al.*, Controllable morphology $CoFe_2O_4$/g-C_3N_4 p–n heterojunction photocatalysts with built-in electric field enhance photocatalytic performance, *Renewable Sustainable Energy Rev.*, 2022, **306**, 121107.

96 J. Zou, W. Deng, J. Jiang, *et al.*, Built-in electric field-assisted step-scheme heterojunction of carbon nitride-copper oxide for highly selective electrochemical detection of p-nonylphenol, *Electrochim. Acta*, 2020, **354**, 136658.
97 Y. Cai, Y. Feng, *et al.*, Review on charge transfer and chemical activity of TiO_2: mechanism and applications, *Prog. Surf. Sci.*, 2016, **91**(4), 183–202.
98 J. Borges, R. Pereira, M. S. Rodrigues, *et al.*, Broadband Optical Absorption Caused by the Plasmonic Response of Coalesced Au Nanoparticles Embedded in a TiO_2 Matrix, *J. Phys. Chem. C*, 2016, **120**(30), 16931–16945.
99 Z. Liu, W. Hou, P. Pavaskar, *et al.*, Plasmon resonant enhancement of photocatalytic water splitting under visible illumination., *Nano Lett.*, 2011, **11**(3), 1111–1116.
100 Y. Wei, *Controlling synthesis of noble metal nanocomposites and their electrocatalytic properties*, University of Jinan, 2019.
101 Y. Hayashido, S. I. Naya and H. Tada, Local Electric Field-Enhanced Plasmonic Photocatalyst : Formation of Ag Cluster-Incorporated AgBr Nanoparticles on TiO_2, *J. Phys. Chem. C*, 2016, **120**(35), 19663–19669.
102 K. Wang, *Study on construction of micro-electric field and property of photocatalyst*, Fuzhou University, 2018.
103 S. K. Dishing, J. Li, F. Meng, *et al.*, Photocatalytic activity enhanced by plasmonic resonant energy transfer from metal to semiconductor., *J. Am. Chem. Soc.*, 2012, **134**(36), 15033–15041.
104 W. Hou, Z. Liu, P. Pavaskar, *et al.*, Plasmonic enhancement of photocatalytic decomposition of methyl orange under visible light, *J. Catal.*, 2011, **277**(2), 149–153.
105 T. Torimoto, H. Horibe, T. Kameyama, *et al.*, Plasmon-Enhanced Photocatalytic Activity of Cadmium Sulfide Nanoparticle Immobilized on Silica-Coated Gold Particles, *J. Phys. Chem. Lett.*, 2015, **2**(16), 2057–2062.
106 A. Nitzan and L. E. Brus, Theoretical model for enhanced photochemistry on rough surfaces, *J. Chem. Phys.*, 1981, **75**(5), 2205–2214.
107 L. Brus, Noble metal nanocrystals: plasmon electron transfer photochemistry and singlemolecule Raman spectroscopy, *Acc. Chem. Res.*, 2008, **41**(12), 1742–1749.
108 X. Chen, H. Zhu, J. Zhao, *et al.*, Visible-Light-Driven Oxidation of Organic Contaminants in Air with Gold Nanoparticle Catalysts on Oxide Supports, *Angew. Chem.*, 2008, **120**(29), 5433–5436.
109 B. Lu, A. Liu, H. Wu, *et al.*, Hollow Au-Cu_2O-Core-Shell Nanoparticles with Geometry-Dependent Optical Properties as Efficient Plasmonic Photocatalysts under Visible Light, *Langmuir*, 2016, 3085.
110 J. Li, S. K. Cushing, J. Bright, *et al.*, Ag@Cu_2O Core-Shell Nanoparticles as Visible-Light Plasmonic Photocatalysts, *ACS Catal.*, 2013, **3**(1), 47–51.
111 N. Nakajima, H. Kato, *et al.*, Photoemission study of the modification of the electronic structure of transition-metal overlayers on TiO_2 surfaces III. Ni on TiO_2 (001) and Cu on TiO_2 (110), *Surf. Sci.*, 2004, **561**(1), 79–86.
112 Z. Jiang, W. Zhang, L. Jin, *et al.*, direct XPS evidence for charge transfer from a reduced rutile TiO_2 (110) surface to au clusters, *J. Phys. Chem. C*, 2007, **111**(33), 12434–12439.
113 D. Panayotov, M. Mcentee, S. Burrows, *et al.*, Infrared studies of propene and propene oxide adsorption on nanoparticulate Au/TiO_2, *Surf. Sci.*, 2016, **652**, 172–182.
114 Y. Cai, M. Zhou, M. Zeng, *et al.*, Adsorbate and defect effects on electronic and transport properties of gold nanotubes, *Nanotechnology*, 2011, **22**(21), 215702.
115 M. Ebrahimzadeh, *Study of the optical properties of nanoparticles using Mie theory*, 2015.
116 X. Jia, J. Shen and H. Yu, Calculation of generalized Lorenz-Mie theory based on the localized beam models, *J. Quant. Spectrosc. Radiat. Transfer*, 2016, S0022407316304460.
117 S. Qu, *Modeling the influences of metallic nanoparticles on the solar energy absorption and photocatalytic properties of TiO_2*, University of Science and Technology of China, 2018.
118 R. L. Aggarwal, L. W. Farrar and S. K. Saikin, Increase of SERS Signal Upon Heating or Exposure to a High-Intensity Laser Field: Benzenethiol on an AgFON Substrate, *J. Phys. Chem. C*, 2012, **116**(116), 16656.
119 X. Chong, N. Jiang, Z. Zhang, *et al.*, Plasmonic resonance-enhanced local photothermal energy deposition by aluminum nanoparticles, *J. Nanopart. Res.*, 2013, **15**(6), 1678.
120 Y. Zhu, W. Yao and R. Zong, *Photocatalysis: application on environmental purification and green energy*, Chemical Industry Press, 2015, vol. 24.
121 D. Li, Y. Huang, S. Li, *et al.*, Thermal coupled photoconductivity as a tool to understand the photothermal catalytic reduction of CO_2, *Chin. J. Catal.*, 2020, **41**(1), 169–178.
122 G. V. Hartland, Optical studies of dynamics in noble metal nanostructures, *Chem. Rev.*, 2011, **111**(6), 3858–3887.
123 Y. Li, *Study on photothermocatalysis with typical oxide photocatalysts*, Northeast Normal University, 2020.
124 X. Fu, L. A. Clark, W. A. Zeltner, *et al.*, Effects of reaction temperature and water vapor content on the heterogeneous photocatalytic oxidation of ethylene, *J. Photochem. Photobiol., A*, 1996, **97**(3), 181–186.
125 Y. T. Lin, C. H. Weng, H. J. Hsu, *et al.*, Effect of oxygen, moisture, and temperature on the photo oxidation of ethylene on N-doped TiO_2 catalyst, *Sep. Purif. Technol.*, 2014, **134**, 117–125.
126 Y. Yi, Y. Li, Z. Qian, *et al.*, Novel photoactivation and solar-light-driven thermocatalysis on ε-MnO_2 nanosheets lead to highly efficient catalytic abatement of ethyl acetate without acetaldehyde as unfavorable by-product, *J. Mater. Chem. A*, 2018, **6**, 14195–14206.
127 X. Xie, Y. Li, Y. Yang, *et al.*, UV-Vis-IR driven thermocatalytic activity of OMS-2/SnO_2 nanocomposite significantly enhanced by novel photoactivation and synergetic photocatalysis-thermocatalysis, *Appl. Surf. Sci.*, 2018, **462**(31), 590–597.
128 F. Liu, M. Zeng, Y. Li, *et al.*, UV-Vis-Infrared Light Driven Thermocatalytic Activity of Octahedral Layered Birnessite

Nanoflowers Enhanced by a Novel Photoactivation, *Adv. Funct. Mater.*, 2016, **26**(25), 4518–4526.

129 L. Zhu, M. Gao, C. Peh, *et al.*, Solar-driven photothermal nanostructured materials designs and prerequisites for evaporation and catalysis applications, *Mater. Horiz.*, 2018, **5**, 323–343.

130 M. Ghoussoub, M. Xia, P. N. Duchesne, *et al.*, Principles of photothermal gas-phase heterogeneous CO_2 catalysis, *Energy Environ. Sci.*, 2019, **12**, 1122–1142.

131 X. Meng, T. Wang, L. Liu, *et al.*, Photothermal Conversion of CO_2 into CH_4 with H_2 over Group VIII Nanocatalysts: An Alternative Approach for Solar Fuel Production, *Angew. Chem.*, 2015, **53**(43), 11478–11482.

132 A. O. Govorov and H. H. Richardson, *Generating heat with metal nanoparticles we describe recent studies on photothermal effects using colloidal*, 2007.

133 A. O. Govorov, Z. Wei, T. Skeini, *et al.*, Gold nanoparticle ensembles as heaters and actuators: melting and collective plasmon resonances, *Nanoscale Res. Lett.*, 2006, **1**(1), 84–90.

134 W. Huang, W. Qian and M. A. El-Sayed, Photothermal reshaping of prismatic Au nanoparticles in periodic monolayer arrays by femtosecond laser pulses, *J. Appl. Phys.*, 2005, **98**(11), 4321.

135 B. Wang, *Study on localized surface plasmon resonance characteristics of metallic bowtie nanoantenna arrays and their applications*, University of Chinese Academy of Sciences, 2020.

136 X. Liu, *Applications of surface plasmon resonance in metal nanoparticles/transparent polyimide composite film*, Huazhong University of Science & Technology, 2019.

137 J. Yu, *Sodium as a plasmonic material: fabrication, properties and applications*, Nanjing University, 2019.

138 J. Luan, *Research on surface plasmon resonance characteristics of silver nanoparticles*, Changchun University of Science and Technology, 2013.

139 C. Tira, D. Tira, T. Simon, *et al.*, Finite-Difference Time-Domain (FDTD) design of gold nanoparticle chains with specific surface plasmon resonance, *J. Mol. Struct.*, 2014, **1072**, 137–143.

140 P. Christopher, H. Xin, A. Marimuthu, *et al.*, Singular characteristics and unique chemical bond activation mechanisms of photocatalytic reactions on plasmonic nanostructures, *Nat. Mater.*, 2012, **11**(12), 1044–1050.

141 L. Gunnarsson, T. Rindzevicius, *et al.*, Confined Plasmons in Nanofabricated Single Silver Particle Pairs: Experimental Observations of Strong Interparticle Interactions, *J. Phys. Chem. B*, 2005, **109**(3), 1079–1087.

142 F. Wu, Y. Du, S. Lv, *et al.*, DFT Modeling of CO_2 Adsorption and $HCOO^{\bullet}$ Group Conversion in Anatase Au-TiO_2-Based Photocatalysis, *ACS Omega*, 2022, 7179–7189.

143 G. Y. Yao, Z. Y. Zhao, Q. L. Liu, *et al.*, Theoretical calculations for localized surface plasmon resonance effects of Cu/TiO_2 nanosphere: generation, modulation, and application in photocatalysis, *Sol. Energy Mater. Sol. Cells*, 2020, **208**, 110385.

144 M. Liu, *Modulating the absorption and near field properties of Au-TiO_2 nanohybrids for photocatalytic application*, Jiangsu University, 2020.

145 W. Zhang, *Research on the photothermal properties of metal nanoparticles*, Zhejiang University, 2014.

146 X. Li, *Researching the extinction properties of noble metal nanoparticles via Discrete Dipole Approximation*, Xiamen University, 2003.

147 L. Shi, *Studying the extinction properties of silver nanoparticles using a method known as the discrete dipole approximation(DDA)*, Jilin University, 2005.

148 F. Yang, *Discrete dipole approximation-guided local surface plasmon resonance enhanced up-conversion fluorescence*, Xidian University, 2020.

149 P. J. Flatau and B. T. Draine, Light scattering by hexagonal columns in the discrete dipole approximation, *Opt. Express*, 2014, **22**(18), 21834.

150 B. Wang, *Investigation on the optical characteristics of magnetite and its nano composites with gold and silver*, Harbin Institute of Technology, 2015.

151 W. He, X. Huang, X. Ma, *et al.*, Significant temperature effect on the LSPR properties of noble metal nanoparticles, *J. Opt.*, 2022, **51**, 142–153.

152 F. Yang, *Precise structure control of TiO_2 composite materials and its photocatalytic performance*, University of Science and Technology of China, 2020.

153 Q. Zhang, *Synthesis and photocatalytic activity study of plasmon enhanced upconversion luminescence photocatalysis composites*, Chongqing University, 2018.

154 T. H. Tan, J. Scott, Y. H. Ng, *et al.*, Understanding Plasmon and Band Gap Photoexcitation Effects on the Thermal-Catalytic Oxidation of Ethanol by TiO_2-Supported Gold, *ACS Catal.*, 2017, 1870–1879.

155 Y. Yang, X. Zhang, C. Niu, *et al.*, Dual-channel charges transfer strategy with synergistic effect of Z-scheme heterojunction and LSPR effect for enhanced quasi-full-spectrum photocatalytic bacterial inactivation: new insight into interfacial charge transfer and molecular oxygen activation, *Appl. Catal., B*, 2020, **264**, 118465.

156 Q. Liu, J. Huang, L. Wang, *et al.*, Unraveling the Roles of Hot Electrons and Cocatalyst toward Broad Spectrum Photocatalytic H_2 Generation of g-C_3N_4 Nanotube, *Sol. RRL*, 2020, **5**(6), 2170063.